

A physics-engineering-economic model coupling approach for estimating the socio-economic impacts of space weather scenarios

Edward J. Oughton¹, Dennies K. Bor¹, Michael Wiltberger², Robert Weigel¹, C. Trevor Gaunt³, Ridvan Dogan¹, Liling Huang¹

¹George Mason University, Fairfax, VA, USA.

²National Center for Atmospheric Research, Boulder, CO, USA.

³Dept. of Electrical Engineering, University of Cape Town, Cape Town, South Africa.

*Corresponding author: Edward J. Oughton (e-mail: eoughton@gmu.edu)

Address: College of Science, George Mason University, 4400 University Drive, Fairfax, VA

Abstract

There is growing concern about our vulnerability to space weather hazards and the disruption critical infrastructure failures could cause to society and the economy. However, the socio-economic impacts of space weather hazards, such as from geomagnetic storms, remain under-researched. This study introduces a novel framework to estimate the economic impacts of electricity transmission infrastructure failure due to space weather. By integrating existing geophysical and geomagnetically induced current (GIC) estimation models with a newly developed geospatial model of the Continental United States power grid, GIC vulnerabilities are assessed for a range of space weather scenarios. The approach evaluates multiple power network architectures, incorporating input-output economic modeling to translate business and population disruptions into macroeconomic impacts from GIC-related thermal heating failures. The results indicate a daily GDP loss from \$6 billion to over \$10 billion. Even under conservative GIC thresholds (75 A/ph) aligned with thermal withstand limits from the North American Electric Reliability Corporation (NERC), significant economic disruptions are evident. This study is limited by its restriction to thermal heating analysis, though GICs can also affect the grid through other pathways, such as voltage instability and harmonic distortions. Addressing these other failure mechanisms need to be the focus of future research.

Key Words

Space Weather, GIC, Power Network, Input-Output Model, Economic Impact

1. Introduction

Variations in the sun-earth space environment negatively affect the engineered systems supporting society and enabling our economy (Gopalswamy, 2022; Manda and Chambodut, 2020; NOAA, 2024). Indeed, space weather is driven by solar activity where periodically transient materials are ejecting into the solar atmosphere in the form of solar flares, High-Speed Streams (HSS), Coronal Mass Ejections (CMEs), and Solar Energetic Particles (SEPs) (Riley et al., 2017; Singh et al., 2021). These events lead to radio blackouts, largely associated with solar flares, geomagnetic storms (e.g., from CMEs), and solar radiation storms (SEPs) (Eastwood et al., 2017; NOAA, 2023).

National Oceanic and Atmospheric Administration (NOAA) measurement scales provide an intensity level for space weather events from 1 (minor) to 5 (extreme). At the more extreme end, storm levels 4 and 5 are classified as natural hazards that pose significant risks to critical engineered civilian and defense infrastructure systems and human lives (MacAlester and Murtagh, 2014). While many scientific studies focus on the physics of space weather and the critical infrastructure impacts, there is still scant literature rigorously investigating the potential socio-economic impacts of space weather resulting from critical infrastructure failure. Indeed, assessing space weather risks to critical national infrastructure and the downstream impacts on society and the economy, is essential for formulating strategic policies to mitigate our shared risk. Such information is essential to support effective decisions for the resilient design of critical infrastructure.

In the United States, a holistic cross-government policy approach was first outlined in the 2015 National Space Weather Strategy and Action Plan, cementing the importance of this topic across relevant federal agencies (SWORM, 2015). Similar policy initiatives are present in other countries ranging from European nations to New Zealand. In 2019, a revised US National Space Weather Strategy and Action Plan was outlined by the Space Weather Operations, Research, and Mitigation (SWORM) Subcommittee (SWORM and NSTC, 2019), with most recently a five-year roadmap being defined for implementing the 2019 National Space Weather Strategy and Action Plan (SWORM, 2023). Importantly, Objective 1.5 outlines the need for improved assessment of the cost of space weather on critical infrastructure, motivating this research.

There are multiple limitations of the research previously carried out on this topic. For example, most assessments provide relatively deterministic estimates of the impacts, such as for electricity transmission failure resulting from a Geomagnetic Disturbance (GMD) (Forbes and St. Cyr, 2004; Schulte et al., 2014). Moreover, many studies have highly stylized approaches to physical hazards, with no model coupling of hazard models, engineered infrastructure systems, and downstream economic impacts. Additionally, previous work estimating daily Gross Domestic Product (GDP) losses resulting from disruption to electricity transmission infrastructure failure rely on an over simplified approach, treating every state's power grid as electrically independent (Oughton et al., 2017).

Thus, our approach in this assessment is to overcome these deficiencies by (i) incorporating uncertainty estimation into potential direct and indirect GDP impacts, and (ii) providing a more logical and improved representation of US power system dependencies which often transcend several states. Subsequently, we provide a novel method to undertake assessment of Geomagnetically Induced Currents (GICs) on the US power grid, by integrating a geoelectric model, a new nationwide electricity transmission infrastructure model, and a macroeconomic model. In our approach we articulate the following research questions:

- 1 Using open-source data, what is the structure of the US electricity transmission infrastructure network?
- 2 How vulnerable is the US electricity transmission infrastructure network under different space weather scenarios?
- 3 What are the potential socio-economic impacts for different space weather scenarios in terms population disruption and lost GDP?

2. Literature Review

This literature review provides an overview of space weather phenomena, the potential effects on critical infrastructure, and then examines past studies quantifying socio-economic impacts. Finally, various macroeconomic modeling techniques are examined, particularly with reference to natural hazards and disaster impact assessment.

2.1 Solar events determining adverse space weather conditions

Variability in the sun's magnetic activity leads to two transient emissions: high-speed solar streams from coronal holes (Younas et al., 2022) and CMEs from bipolar magnetic regions (sunspots). The emitted solar plasma travels through space and the interplanetary medium, interacting with the background solar wind, forming shock sheaths for CMEs (Kilpua et al., 2017; Webb and Howard, 2012) and stream interaction regions for HSS. The physical interactions lead to the acceleration of SEPs and high-energy solar flares (Gopalswamy, 2022). These activities typically intensify during solar maximum (Bhowmik et al., 2022).

CMEs are large-scale transient events from the sun characterized by the ejection of fast-moving plasma and magnetic fields into space. A CME's severity is determined by its internal magnetic fields, mass, and speed. The speed typically ranges from 20 km/s to 3000 km/s (Riley et al., 2017). CMEs are the main drivers of space weather events leading to geomagnetic storms, accelerating charged particles, and ground-level enhancements (Firoz et al., 2010; Gopalswamy, 2016).

2.2 Critical infrastructure impacts

While there are multiple definitions of what constitutes critical infrastructure (Hall et al., 2017; Oughton et al., 2018), a commonly used definition refers to the 16 critical infrastructure sectors identified by the US Department for Homeland Security (DHS), including communications, energy, and transportation sectors (CISA, 2024). Here, we focus on electricity transmission infrastructure and Extra High Voltage (EHV) transformers in relation to exposure to GICs.

During a severe geomagnetic storm, the dayside of the Earth's magnetosphere is compressed by either one or multiple high-speed traveling CMEs (Ganushkina et al., 2018; Hajra, 2022). If the incoming CME's magnetic field is southward oriented, magnetic reconnection may occur between the CME and Earth's magnetic field, leading to energy dissipation into Earth's magnetosphere. Charged particles, including plasma ions and electrons injected from the CME, subsequently drift along Earth's magnetic field lines to the polar regions. The induced energy enhances atmospheric ring currents primarily comprised of ions and electrons. Ring currents are toroidal in shape and rotate westwards, and due to their covariance with the local horizontal magnetic field, are a good measure of Disturbance Storm-Time (Dst) (Banerjee et al., 2012).

The energy deposited in the upper atmosphere causes ionospheric perturbations, leading to spatially and temporally varying local magnetic fields (Oliveira and Ngwira, 2017; Pulkkinen et al., 2017). This induces an electric current into the ground infrastructure by Faraday's law of induction (Piersanti et al., 2019). GICs are low-frequency (0.001 to 0.1 Hz) quasi-dc currents with amplitudes of 10-15 A and peaking at 300 A for 1-2 mins periods (Abda et al., 2020; Albert et al., 2019).

When GICs flow in a transformer, it introduces non-linearities, causing a phase shift of the sinusoidal wave. They cause half-cycle saturation due to a non-linear response to the transformer core material (Klauber et al., 2020). The aftermath is harmonic saturation and increased transformer magnetizing power (Taran et al., 2023). Moreover, GICs in power lines cause malfunctioning of relays (Rajput et al., 2021), excess heating in capacitor banks, and an increase in reactive power consumption (Heyns et al., 2021; Hughes et al., 2022; Wang et al., 2020). This reduces the age of the transformer and may cause permanent damage.

In a worst-case scenario, a voltage collapse may lead to a loss of power across the grid (raising challenges in black-starting the network). In some circumstances, safety equipment may lead to grid assets 'tripping off' automatically, which can also lead to cascading failure and a loss of power. The intensity of GIC is dependent on the spatial-temporal aspects of magnetic fields, the geometry of the ground infrastructure, and the conductivity of Earth (Dimmock et al., 2019; Gritsutenko et al., 2023; Kataoka and Ngwira, 2016; Kelbert, 2020). Ground inhomogeneities and proximity to coastal regions drive induced E-fields of varying magnitudes (Heyns et al., 2021).

2.3. Socio-economic impacts

Business activities can be affected by space weather events due to disruptions to electricity supply, telecommunication systems, as well as other necessary critical infrastructure services (Miteva et al., 2023; Oughton, 2021; Xue, 2023; Xue et al., 2023). Famously, the 1989 geomagnetic storm caused significant disruption to the Hydro-Quebec electricity transmission grid. The event triggered safety mechanisms on the power system to protect transformer assets, leading to a severe and widespread blackout that caused as much as US \$6.5 million in equipment damage and US \$13.2 million in economic losses (Cander, 2019).

Studies have highlighted the importance of mitigating the potential impacts of a Carrington-sized space weather event in Europe. These studies advocate for the implementation of a space situational awareness program to enhance space weather data collection and forecasting capabilities (Oughton et al., 2019). Both the direct and indirect impacts of such an event are considered over a 1–3-month window, including the cascading pathways through which damage could propagate. The researchers determined that a large-scale space weather event could cause as much as €21 billion (US \$22 billion) in damages by 2024, including €1.1 billion (US \$1.2 billion) from spacecraft design and operations, €11.1 billion (US \$12 billion) in aviation losses, €6.4 billion (US \$6.9 billion) from power grid operations, and €1.8 billion (US \$1.9 billion) in logistical and road transportation losses. However, these significant economic impacts could be mitigated through space weather situational awareness, potentially saving €3.5 billion (US \$3.8 billion) annually by 2024 (Luntama and others, 2017).

Additionally, a global supply chain assessment found that an event like the Quebec 1989 storm taking place over the Americas, could reduce consumption by 3.9% in the western hemisphere while possibly increasing consumption in other countries such as France, Egypt and Saudi Arabia (due to price changes and supply chain reconfiguration) (Schulte et al., 2014). The authors estimate that an extreme storm could cause annual

GDP losses up to US \$3.4 trillion, or about 5.6% of the global economy. These numbers are based on numerous strong assumptions which elevate the impacts to one of the worst natural disasters in modern history. These assumptions are simplistic and are not based on direct coupling of physics and engineering models. Focusing on Japan, a quantitative evaluation of the macroeconomic impacts of space weather considers a range of effects to understand how society might be affected. The analysis concluded that simulated storm events could cause Japan to incur losses between ¥19.8-23.8 billion (US \$130 million to \$160 million) per day due to a myriad of failures, including electricity, navigation, and radio communication (Ishii et al., 2021).

The findings from research utilizing North American insurance data indicates a relationship between equipment loss insurance claims and geomagnetic activity. The study focused on establishing a correlation between geomagnetic activity and claim rates, finding that 20% more claims were filed on days with the top 5% space weather activity. The researchers further established the correlative relationship between geothermal activity and insurance claims for the malfunction of electronic equipment, over 59% of which were attributed to electrical surges. The study found that the storms could cause upwards of US \$188 billion annually for businesses across the United States (Schrijver et al., 2014).

Space weather events affect the cost of electricity, and as shown by a study in China using the value at risk model, the electricity demand increased due to space weather. Consequently, electricity consumption increased with solar, wind, and geomagnetic indices at household and industrial levels (Wu et al., 2021). Applying a simulated storm event in China, an equivalent to a March 1989 storm, would have a higher probability of damaging power infrastructure (Zhang et al., 2022). Moreover, analysis of Canada indicates space weather activity leads to lower output of consumption and investment, causing loss of 0.26% in GDP per capita (Zhao, 2019).

Space Weather poses a significant threat to critical infrastructure across the world (Taylor, 2020). When meteorological systems, navigation systems, and communication are interrupted, there are significant consequences for those who rely on those systems. Research has indicated that contemporary critical infrastructure is not prepared to handle or mitigate extreme space weather events (Botezatu, 2023; Dickinson and Gannon, 2023; Facsko et al., 2023; Kolarski et al., 2023). As demonstrated with the aforementioned research, the potential socio-economic impacts are extreme, threatening international communication, the macroeconomic supply-chain, and power grid accessibility (Baum, 2023; Nowakowski et al., 2023).

2.4 Macroeconomic disaster risk modeling methods

Failure of critical infrastructure can result in significant lost value-added activities to the economy, via shocks to supply chains that support economic production, distribution, and consumption. A natural disaster or similarly devastating event can temporarily interrupt or permanently discontinue an industry's access to input goods and services, as well as preventing the downstream selling of goods and services. There are multiple different ways to model the GDP impacts of infrastructure failure, from Input-Output (IO) to general equilibrium approaches (Galbusera and Giannopoulos, 2018; Kelly, 2015a; Sue Wing and Rose, 2020).

The IO approach is distinguished by the Leontief method for estimating upstream demand-side effects and the Ghosh method for assessing downstream supply-side impacts. While there are certain limitations to this

group of methods (Oosterhaven, 1988; Rose and Casler, 1996), which rely on an assumption of sectoral inflexibility, IO approaches provide the advantage of enabling macroeconomic sectoral interdependencies to be quantified (de Santana Ribeiro et al., 2023; Kelly, 2015b; Pamucar et al., 2023; Sarkar and Gupta, 2023). Consequently, providing useful risk analysis insight from the potential failure of certain linkages between industrial sectors supported by infrastructure assets. It is also possible to quantify GDP impacts arising from disruption to a national economy.

As a disaster causes a cascading economic effect throughout a national economic structure, its GDP impacts can be classified into two unique categories (Lin et al., 2017; Rocchetta, 2022). A sector's disturbance can cause 1) downstream economic impacts on industries that rely on that sector's goods as an input or 2) upstream economic impacts on industries that the sector relies on for input goods (Chen et al., 2009; Setola et al., 2009; Soon et al., 2019; Zorn et al., 2020). IO modeling can measure the domino effect of upstream and downstream impacts by combining the Leontief IO models and Ghosh IO models (Sprintson and Oughton, 2023). The Leontief and Ghosh IO models can be used to empirically study the effects of natural disasters, which influence the economy by straining or destroying critical infrastructure (Botzen et al., 2019).

One study used an IO model to study the critical infrastructure failures associated with Hurricane Sandy. Separating the economy into 71 sectors, following the distinctions made by the North American Industrial Classification System (NAICS) system, the paper reported an estimated loss of US \$36 billion (Santos et al., 2023). Another study employed an IO approach to estimate the indirect losses for constituent sectors of the Chinese economy following flooding in the Jiangxi province. The study also separated the economy into sectors and analyzed the indirect effects associated with the interdependencies. Predicting a multiplier of 2.08, wherein the indirect losses are 2.08 times the direct losses, the paper predicted a loss of CNY 177 million (US \$24.94 million) for the manufacturing sector. With the paper employing a Multi-regional IO model, it could more closely analyze the damage within the context of the Jiangxi province, which might have different market interdependencies than the nationwide market (Lyu et al., 2023).

Similarly, IO methodology can be used to study the supply chain impacts of earthquakes, as one study did for the Sichuan earthquake of 2008. A multi-regional IO table was constructed and fed information about final demand changes and value-added losses. The paper found that the earthquake caused up to US \$1,725 billion in losses, centered around the Chemical industry in Southeast China. With the IO table enabling impacts to be reported by macroeconomic sector, this allowed the researchers to isolate the effects of the disaster by industry, thus analyzing ripple effects throughout the economy (Huang et al., 2022).

There are other augmentations of the Leontief and Ghosh IO approaches used to study critical infrastructure failures. For example, it is possible to utilize an IO approach to focus on topological analysis of the interdependency network to identify systemic vulnerability across industrial sectors (Chopra and Khanna, 2015). Moreover, it is possible to implement dynamic IO modeling, to estimate how the market would likely reach equilibrium after a critical infrastructure failure (Jonkeren and Giannopoulos, 2014). One study used the general equilibrium model to analyze weather shocks to the economy, predicting how market forces would eventually decrease consumption by as much as 5.3% in countries prone to weather disasters (Cantelmo et al., 2023). Significant attention has been given to the need for creating a larger and more reliable dataset for IO analysis (Hasan and Foliente, 2015).

These IO methods contrast with other methods for analyzing the effects of critical infrastructure failure, whether that might be a more geospatial approach (Koks et al., 2019), adapting probabilistic risk analysis tools (Deng et al., 2020), or developing Bayesian techniques to quantify infrastructure interdependency (Hossain et al., 2020).

We now present a method which enables us to answer the key research questions.

3. Method

This section outlines the framework used for vulnerability assessment of the contiguous US power grid. A novel geospatial framework has been developed to model power load flow by integrating existing geophysical models to estimate GICs flowing through transformers and grounded substation points. The power system's response is analyzed under varying thermal thresholds for diverse space weather events to identify substations where transformers are at risk. Finally, a stochastic Monte Carlo modeling approach is utilized to evaluate the direct and indirect economic costs incurred for different magnitudes of space weather scenarios. Figure 1 indicates the physics-engineering-economic model coupling method utilized.

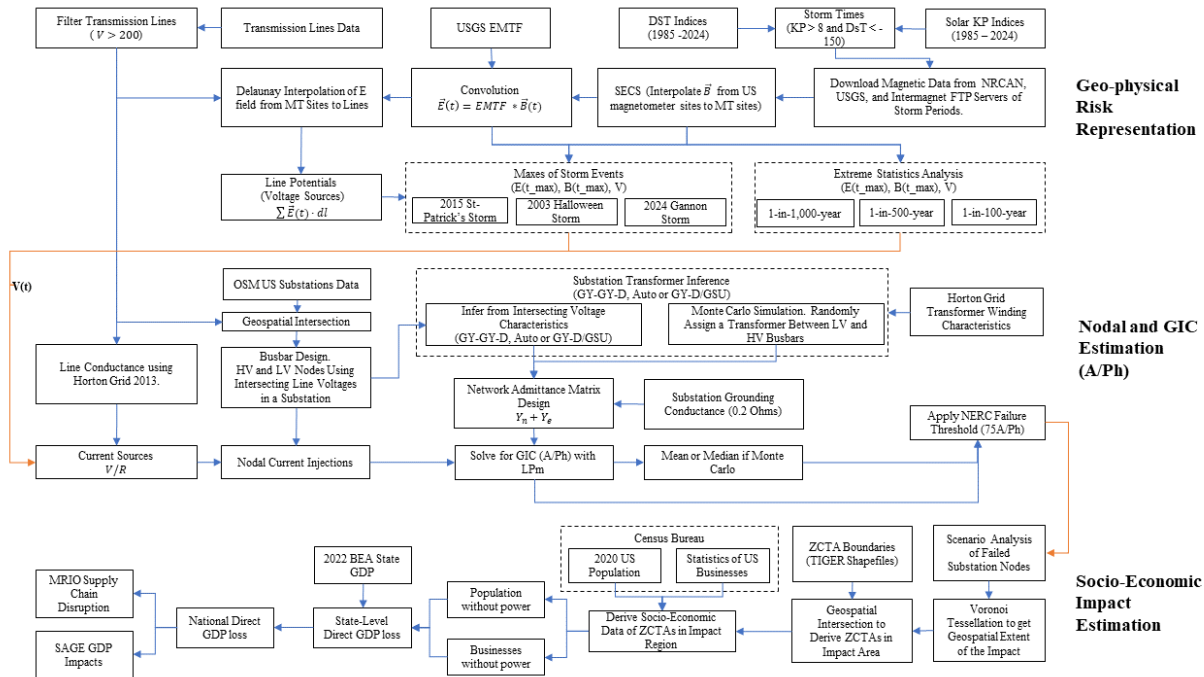


Figure 1. Method Box

3.1 Design of the US power grid network

This section outlines the creation of a geospatial nationwide power grid network for the contiguous United States. Location data for 60,000 substations were acquired from OpenStreetMap (OSM), while transmission line data were sourced from the Homeland Infrastructure-Level Data (HIFLD) (HIFLD, 2023). These datasets were combined using geospatial set theory, intersecting substations (nodes) with transmission lines (edges) to construct the power network. A 250-meter buffer was applied to each substation to enhance the

accuracy of intersections. Only substations and transmission lines with a voltage rating of 230 kV or higher were used in the study (Oughton, 2024).

We set up two cases to estimate the transformer type in a substation: (i) a deterministic method based on the voltage ratings of the intersecting transmission lines, where each substation is assumed to contain a single transformer, and (ii) a stochastic method that simulates the network under varying transformer configurations. In the deterministic case, the transformer type is identified based on the voltage characteristics of the geospatially intersected transmission lines. This framework enables the design of both low-voltage and high-voltage buses.

The transmission line attributes include the voltage ratings. The number of unique voltage ratings is applied to estimate the substation bus count. The busbars are Points of Common Coupling (PCC) for line bays, transformer bays, reactor bays, capacitor banks, Flexible AC Transmission Systems (FACTS) devices, and switches used to re-configure (couple or split) a busbar. Power transformers are connected to two busbars or occasionally to three busbars. For example, via the primary and secondary windings of substation transformers or as taps for the connections to other substation buses.

The standard voltages for transmission in the US are 161, 230, 345, 500 and 765 kV. For economic reasons, the transformer has a Wye winding at these voltages. The neutral point of the Wye winding is usually grounded, where GICs enter and leave a system. Lines of 115 and 138 kV are typically classed as distribution, which are rarely long and have smaller, higher resistance conductors. Thus, the GICs in systems operating at these voltages are very often neglected (although not exclusively). In this power model, three considerations are made for different types of substations.

Firstly, generator substations are identified with a generator step-up unit transformer/s (in some generating stations, two generators are connected to one transformer). The transformer windings type is usually a Delta/Wye-grounded transformer. GICs enter the substation through the transmission lines; therefore, no GIC flows in the primary (lower voltage) windings connected to generators. Usually, the lines connected to this substation have the same voltage ratings, but power might be exported at two voltage levels in some generator substations. For this asset type, we expect the substation consists of a single transformer between low-voltage and high-voltage busbars.

Secondly, transmission substations are identified. Most have step-down transformers, with power flow from higher to lower voltages. Some substations have multiple voltage-rating buses. Most transformers are connected by only two busbars. If the ratio of the voltages is less than 2, the transformer may be an autotransformer; if the ratio is higher, the transformer will be a Wye/Wye type with both neutrals grounded. When a 3-winding transformer is connected to three different voltages, it is usually a three-winding Wye-Wye-Delta transformer. The third asset is a switch yard. This configuration is decided based on multiple transmission lines of the same voltage rating connected to the substation, with no lines of other voltages, as well as the node not serving a proximate generating station.

In the second case, involving Monte Carlo simulation of transformer configurations, variability in transformer types and quantities is accounted for by randomly assigning up to four transformer configurations across different scenarios. GICs are calculated for each scenario, and to ensure a representative estimate, 1,000 simulations are analyzed to determine the mean and median GIC per phase at each substation. The use of the mean strikes a balance between computational feasibility and the need for robust estimates, considering the complexity of solving for nodal voltages. These values are

subsequently applied in the vulnerability analysis of specific nodes. For substation transformer configurations, the North American Electric Reliability Corporation (NERC) thermal threshold, as defined in TPL-007-2, sets a conservative limit of 75 A per phase for all transformer variants (NERC, 2017). To assess sensitivity, thresholds of 25, 50, 75, 100, 125, and 150 A per phase are evaluated, and the resulting economic impacts from the associated failures are analyzed. Our methodology builds upon this approach.

3.2 USGS GMD hazard model

The Dst and Kp data from 1985 to August 2024 were downloaded from Kyoto WDC and GFZ Potsdam, respectively (Kyoto, 2024; Matzka et al., 2021). Events with Dst values less than -140 nT or a Kp index greater than eight were selected as qualified storm events. A buffer of 1.5 days before and after the time of the main event was added and used to download a minute resolution of the magnetic field data from Intermagnet (Kerridge, 2001), US Geological Survey (USGS), and National Resource Canada (NRCAN) magnetic file transfer servers (NRCAN, 2024; USGS, 2024). Moreover, the method uses the magnetotelluric data of the entire US from the USGS Earthscope and USArray Magnetotelluric (USMT) campaigns (Kelbert, 2023).

Quantifying the magnitude of the geoelectric currents in ground infrastructure depends on the rate of change of the earth's magnetic field, the earth's conductivity structure, and the topology of the network infrastructure at risk (Rigler et al., 2019). During the phase of the geomagnetic disturbance, there is a significant intensification and fluctuation of the magnetospheric-ionosphere ring currents, which subsequently induce surface geoelectric fields according to Faraday's law of induction.

The estimates of electric fields in the real world are derived from relating time-varying magnetic components measured by magnetometers placed at different locations on the Earth's surface. The recorded fields are interpolated using a Spherical Elementary Current System (SECS) to obtain the magnetic field components at Earth's magnetotelluric sites. The magnetic fields at the impedance sites are convolved with the 3D solid earth conductivity data to obtain geoelectric field components using Equation 1. Thus, the time series magnetic data is convolved into a frequency domain using the Fast Fourier Transform (FFT), then matched with ground impedance to extract the spectra of the electric fields. An inverse fast Fourier transform is applied to obtain the time series of the electric field at the ground stations.

Once the magnetic and geoelectric fields are obtained, the Delaunay tessellation is applied to interpolate the geoelectric field along the transmission lines. Delaunay triangulation assigns weights to the nearest line from each site, and those with the highest weights are considered. The interpolated geoelectric field is integrated over the entire transmission line using Equation 4 to obtain the voltage sources driving GIC in the network.

The frequency of occurrences of space weather events (CMEs, solar flares, solar proton events, etc.) is predicted to fit a power-law distribution. Thus, once the geoelectric field, magnetic field, and voltages induced along the transmission line are obtained, a power law distribution is fitted to extrapolate for the 100, 500, and 1000-year return periods. Similarly, the interpolated voltage values from the peaks of the past recorded storm events, including the 2003 Halloween storm, 2015 St Patrick's storm, and 2024 Mother's Day Gannon storm, are extracted and applied to the power network model.

3.3 GIC estimation via the Lehtinen-Pirjola modified method

Due to its quasi-static nature, the power system can be modeled as a DC circuit comprising line, transformer, and substation ground impedances (Heyns et al., 2020). Reactive impedances have a negligible impact on the system and are therefore ignored (Pirjola et al., 2022). Due to limited information on the transformer and transmission line types, test case values taken from the literature are used to design the system impedances (Horton et al., 2012).

The geoelectric field's vector, derived from its direction on the Earth's surface and the angle formed with the transmission lines, determines the GIC magnitude. The GIC magnitude also depends on the Earth's resistivity and the resistivity of the transmission lines. Excluding ground resistivity from the analysis would significantly reduce the GIC along transmission lines (Boteler and Pirjola, 2017). For a plane wave propagation of the magnetic field, the frequency component of the horizontal geoelectric field ($\vec{E}_h(\omega, x, y)$) is obtained by convolving the frequency component of the magnetic field ($B_h(\omega, x, y)$) with the ground conductivity transfer functions (Z) as illustrated in Equation 1.

$$\vec{E}_h(\omega, x, y) = \frac{1}{\mu} (Z * \vec{B}_h)(\omega, x, y) \quad (1)$$

μ is the permeability of the magnetic field propagation medium.

In modeling GIC in power systems, the current flows through the transformer primaries to the ground through the transformer neutral points. Thus, the type of transformer will determine the GIC flowing within each asset, for example GIC does not flow in Delta-type transformers. GIC (I_{gic}) flowing in localized networks at time t is determined by the characteristics of the nodes a and b as given in Equation 2 where the E_x and E_y are the northward and eastward components of the geoelectric field (Ngwira and Pulkkinen, 2019). This approach considers a uniform northward and eastward geoelectric field.

$$I_{gic}(t) = a\vec{E}_x(t) + b\vec{E}_y(t) \quad (2)$$

The induced geoelectric field along the transmission lines is the driving force of GIC in the transformers to the ground. The voltage sources along the transmission lines are dependent on the magnitude of the induced field and the transmission line length L . This can be obtained by integrating the geoelectric field over a transmission line displacement vector by Equation 3.

$$V = \int \vec{E} \cdot d\vec{l} \quad (3)$$

Where V is the driving electromotive force for time varying geoelectric field, E is the net geoelectric field, and $d\vec{l}$ is the differential line transmission length. This simplified approach is useful when a uniform geoelectric field is considered. However, in the real world, the transmission lines consist of spatial linestring geometry objects traversing a spatially and temporally varying geoelectric field. For each line segment, a uniform geoelectric field is assigned through Delaunay tessellation interpolation from magnetotelluric sites. The electro-potential along each line segment is calculated using Equation 4 where \vec{E}_E and \vec{E}_N represent the eastern and northern components of the geoelectric field, respectively. The total potential difference along the entire transmission line is computed by summing the potentials of each line substring for the eastward

(L_E) and northward (L_N) components. This process can be simplified by averaging geoelectric fields from magnetotelluric sites within a 4.5 by 4.5-degree grid.

$$V = \sum(\vec{E}_E L_E + \vec{E}_N L_N) \quad (4)$$

Given the transmission lines' conductance and V , Ohm's law is applied to estimate the current sources j_{nk} into the nodes n and k using the Equation 5. R , is the resistance of the transmission line.

$$j_{nk} = \frac{V}{R} \quad (5)$$

The Lehtinen Pirjola modified (LPm) method is applied to solve for the nodal voltages and the GIC through the transformer primaries and grounded neutral points of the substations. We begin by summing the currents from equation 5 in the substation busbars to obtain current injections j_k into node k , resulting in a column vector of currents J_e for all the examined busbars and nodes. The admittances comprise the network admittances Y_n and earthing impedances Y_e . Equation 6 is then used to solve nodal voltages.

$$V_n = ([Y_e] + [Y_n])^{-1} [J_e] \quad (6)$$

The resulting system of admittances is a sparse matrix whose diagonal elements are the admittances of a path to the node n while off-diagonal elements are negative admittances of the elements between bus n and k . Moreover, this matrix is positive semi-definite, and its solution can be simplified using LU decomposition. The nodal potential difference that drives the GIC along the transmission lines is solved using the equation 7.

$$i_{nk} = j_{nk} + y_{nk}(v_n - v_k) \quad (7)$$

Where i_{nk} , j_{nk} , y_{nk} are the GIC, current source, and admittances between node n and k , respectively. The v_n , and v_k are the solved voltages in n and k busbars. The current through the grounded neutral points at the node k , is solved using equation 8, where Z_e is the grounding impedance or reciprocal of the earthing admittance.

$$I_e = [Z_e]^{-1} V_n \quad (8)$$

The nodal voltages (at busbars and neutral points) solved using the LPm method are used to compute currents flowing through transformer windings to neutral points and GICs along transmission lines.

Our modeling framework acknowledges the existence of GIC protection systems, such as GIC blocking devices, although we lack data on the substations fitted with these systems (and importantly, there are not that many in current operation). We neglect the GIC flow in secondaries since it generally provides a path for the flow of GIC into the primary of the adjacent substation.

For a number n of transformers with a GIC above a sensitivity threshold from the set, {25, 50, 75, 100, 150} passing through the primaries (or serial winding for autotransformer) we consider that it may fail. A stochastic approach is undertaken in modeling their failures due to the uncertainties in core type, core design (3 or 5 limbs), age, lack of GIC vulnerability data from manufacturers, and lack of substation protection data. Therefore, all the transformers above the defined GIC threshold fail for the pessimistic bound. If robust measures have been undertaken to cushion transformers from GIC, all may withstand the geomagnetic event and not fail.

Moreover, this probabilistic approach to failure estimates accounts for other unknown factors, such as the type of network topology. For example, in a radial network, failure in one unit may affect the adjacent dependent downstream substations. However, grids typically have resilient topologies like ring or mesh configurations. In such cases, a power failure at one node does not necessarily affect the adjacent node and, instead, may stress the network or affect only a tiny portion of the population.

3.4 Socio-economic impact analysis

To estimate potential socio-economic impacts multiple different datasets are required. The primary socio-economic data sources include information from the US 2020 decennial census (Bureau, 2020), the Statistics of US Businesses (SUSB) survey (Bureau, 2023), state-level GDP data from the Bureau of Economic Analysis (BEA) (BEA, 2023a), and BEA supply-use tables (BEA, 2023b). The statistics of US businesses comprise economic data at the US ZIP level. A concordance table is applied to translate the Zip code to the Census Bureau boundary ZIP Code Tabulation Areas (ZCTA). The resulting dataset comprises the number of businesses by the NAICS, total firm employees, regional population, and annual employee remuneration.

A transformer failure in a transmission or distribution substation may lead to the asset's functionality loss, and it may cause power loss to other dependent substations, which could be of transmission or distribution role. When extracting the spatial extent of the effect, we apply a Voronoi tessellation algorithm by taking adjacent substations as centers. For substations at the edges with no other connected substations, a spatial radius of 500 km is considered, with the failed substation as the center. This approach allows the intersection of the spatial cells with ZCTA cartographic shapefiles from the US Census Bureau Tiger Program. The representative points of the ZCTA boundaries within the cells enable the derivation of socio-economic data to extract the impacted businesses and population quantitatively.

In terms of the failure mechanism modeled here, GIC flowing in transformer windings above a selected tolerance value may lead to thermal heating of transformers components and eventual failure, causing loss of service to the businesses and the population being served. When a node fails, we consider a 100% loss of economic output in that area. Since we lack geographic data on the annual population final demand by NAICS, the impact assessment is based on the loss of gross value added, a quantity used by BEA to estimate the GDP of each state. Daily economic losses are reported due to the uncertainties in the duration it takes to restore the power system to normalcy (especially as this is an area of much debate). In the literature, power restoration ranges from a few days to a couple of weeks, depending on the nature of the damage. Hence, the daily focus here.

Our approach to substation failure considers two possible combinations, including fault state 1, which is a 100% loss of power, and fault state 0, where the substation functions nominally. In scenario analysis, for fault 1, Y number of substations fails, where Y is an integer from 1 to n , where n is the number of transformers whose magnitude of GIC values in their primaries surpasses the NERC thermal threshold.

The gross value added by business sector at ZCTA is unfortunately not available. Thus, we devise a set of linear equations that leverage the proportion of businesses counted at ZCTA boundaries to their aggregates at the state level and then compare them with their GDP contribution by business category. For a scenario leading to a failure at a substation x , businesses B and population P are impacted. Thus, the GDP shock $v_{s,x}$ by sector s in an area served by a substation x is:

$$v_{s,x} = \frac{B_{s,x}}{\sum_S B_s} G_s \quad (9)$$

Whereby G_s is the total contribution of the sector s to the state GDP. The denominator $\sum_S B_s$ is the count of business establishments by industry s in the state where the failed substation resides. $B_{s,x}$ refers to business counts by sector s in the area x . The direct impact by sector s for a scenario where Y number of substations malfunction is shown by Equation 10.

$$v_s = \sum_{x \in Y} v_{s,x} \quad (10)$$

Therefore, we end up with a column vector v which is the total economic shock aggregated through the impact regions.

$$v = [v_1, \dots, v_n] \quad (11)$$

Once we have the value-added shocks by sectors, we stochastically generate distributions from different failure scenarios by drawing all possible Y values within set n to establish exceedance probabilities. In this case, we end up with $pow(2, n)$ combinations where values within the 5th, 50th, and 95th percentile are considered. Whereas for scenarios potentially leading to extreme values that may become computationally intensive, we randomly sample a million failures within the possible combinatorics. This is undertaken several times while averaged to extract an almost accurate range of values according to the central limit theorem.

We use the Ghosh model to analyze GDP output from lost inter-industry value-added activities. The model relies on an economy's sectoral decomposition, distinguishing separate industries via NAICS code. By aggregating data related to inter-sectoral demand, we can produce a matrix that satisfies equation 12.

$$x' = v' G \quad (12)$$

Now, x' represents a 1 by n vector representing the GDP shock out of each economic sector, v' is a 1 by n transposed vector representing value-added shocks in 11, and G represents the Ghosh matrix. Through this method, we shock the Ghosh matrix with a loss in value-added activities to estimate the downstream impact of a disruption in the economy resulting from critical infrastructure failure. Ghosh's model presupposes a sectoral analysis of an economy and depends on an assumption of proportional uses of inputs. Within this representation, the method treats the economy as closed, static, and without structural changes responding to the subjected perturbations.

4. Results

This section highlights the results from the coupled physics-engineering-economic modeling approach. These are outlined with respect to the defined research questions: (i) what is the structure of the US power grid, (ii) how vulnerable are these assets under different space weather scenarios, and (iii) what are the potential socio-economic impacts from service loss?

4.1 Using open-source data, what is the structure of the US electricity transmission infrastructure network?

This study focuses on EHV substations in the United States. Recent research has also shown renewed interest in modeling lower voltage sections of the grid, due to the cumulative GIC effects from minor distribution lines feeding into substations. Initially, 1,370 substations (≥ 345 kV) were collected from OSM. Expanding the filters to include those above 230 kV increased the number of distribution and transmission substations to 3,685. The transmission lines connecting these substations are typically longer and have minimal line resistance, enabling maximum GIC flow. Figure 3 shows the filtered transmission lines that connect these 3,685 substations.

The power grid design model comprises 955 substations with autotransformer types and 2,730 grounded Wye types. The Wye category includes Wye-Wye, Generator Step-Up Unit (Delta-Wye), and three-winding grounded Wye-Wye-Delta configurations. Each substation model contains two busbars: a high voltage bus connected to the transformer's primary winding and a low voltage bus connected to the secondary windings for step-down units. The transformer types are determined by the voltage ratings of the buses, a methodology validated by experienced power engineers during the workshop at George Mason University (GMU) in September 2024.

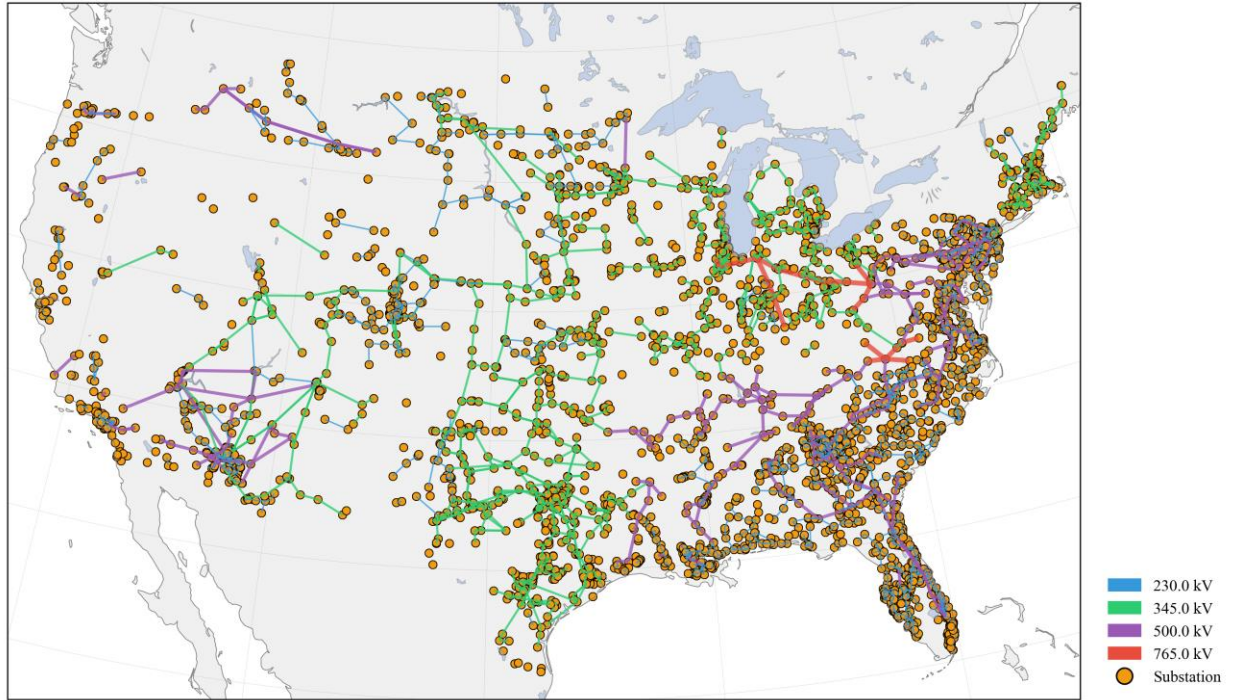


Figure 2. A developed geospatial network of the US power grid by intersecting the open substations data from OSM and HIFLD transmission lines data. The substations and transmissions lines whose voltage ratings are above 200 kV are only considered in this analysis.

4.2 How vulnerable is the US electricity transmission infrastructure network under different space weather scenarios?

We report the extrapolated magnetic, geoelectric, and computed transmission line voltages for 100-, 500-, and 1000-year return period events, derived from past storm period data using a power law distribution. We utilized the BezPy and Powerlaw Python packages for this analysis (Lucas and Erigler-USGS, 2023; Schaefer and Rob, 2017). It is worth noting that some industry experts in the space weather community have expressed reservations about whether these extreme space weather events beyond 100-year return periods truly exhibit power law behavior. Figure 3 shows the geoelectric field results from the power-law fit and the maximum geoelectric field observed during the 2024 Gannon storm.

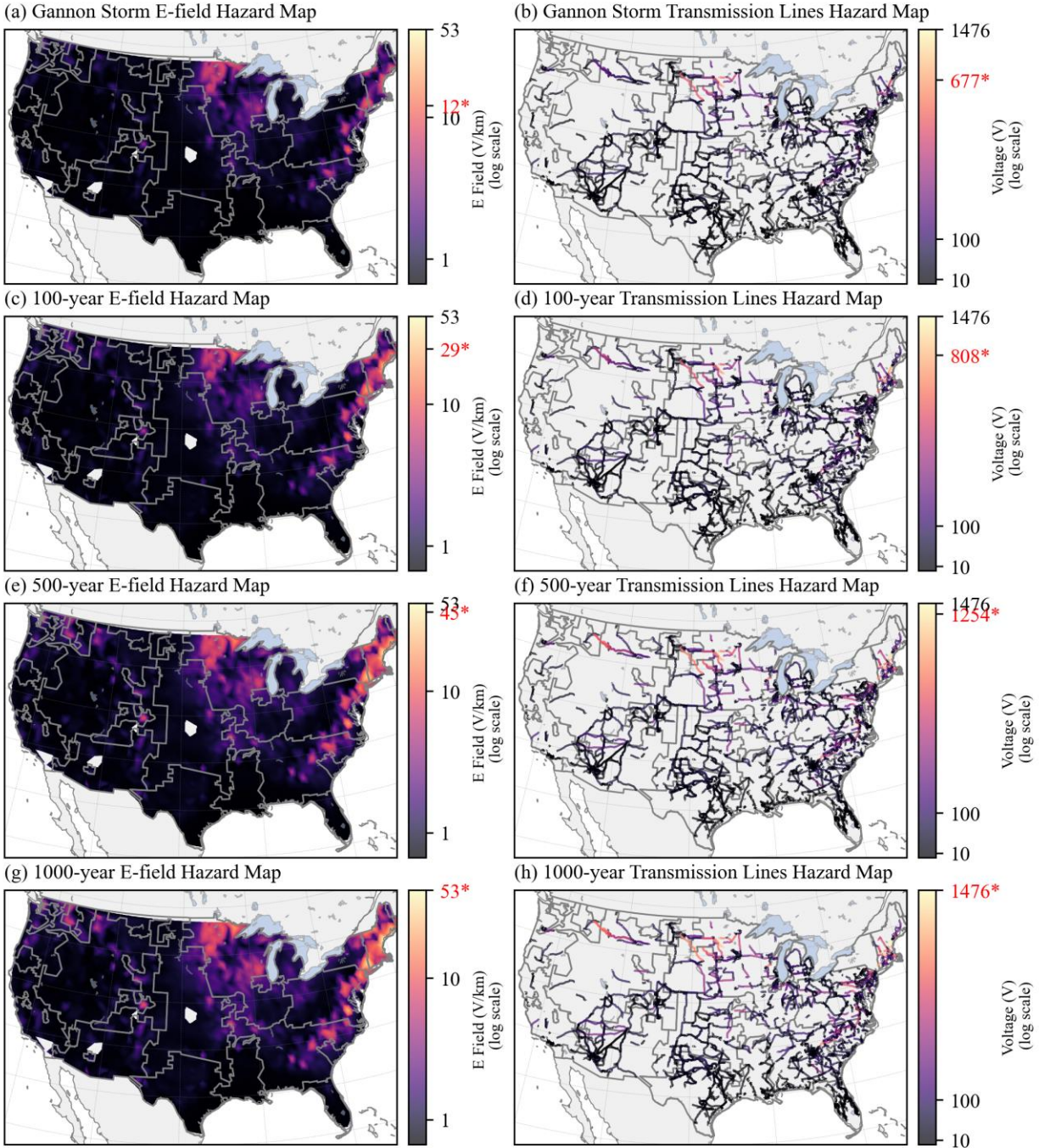


Figure 3. Overview of the May 2024 Gannon storm and extrapolated geoelectric fields and transmission line-induced voltage sources for 100-, 500-, and 1000-year return periods across the contiguous US. The first column shows the geoelectric field interpolated to a 1000 by 1000 grid from US magnetotelluric sites using the nearest neighbor method. The second column presents the summed geoelectric field along EHV transmission lines, interpolated from magnetotelluric sites using the Delaunay triangulation method for each examined scenario.

Maximum geoelectric fields were recorded in the northern states across all reported scenarios. The highest recorded geoelectric field reached 53 V/km for the 1000-year event scenario, though this remains significantly lower than values previously recorded and theorized in literature. A maximum voltage source (electromotive force) of 1.5 kV, the GIC driver, was reported across analyzed scenarios. The intensity of both geoelectric field and induced voltage sources diminishes toward the south.

A maximum geoelectric field of 29 V/km was reported for the 100-year event scenario, aligning with the US geoelectric maps published in literature (Lucas et al., 2020). For the 500-year extreme event return period, a maximum of 45 V/km was obtained. The analysis of transmission lines was filtered to include only EHV lines, which may underestimate the highest voltage sources when compared to a comprehensive analysis including all distribution and transmission lines. These extreme GIC and voltage values were recorded in the upper states of Minnesota, Wisconsin, Indiana, and Pennsylvania. These regions situated closest to the auroral electrojet are known to exhibit the highest electrical ground impedances.

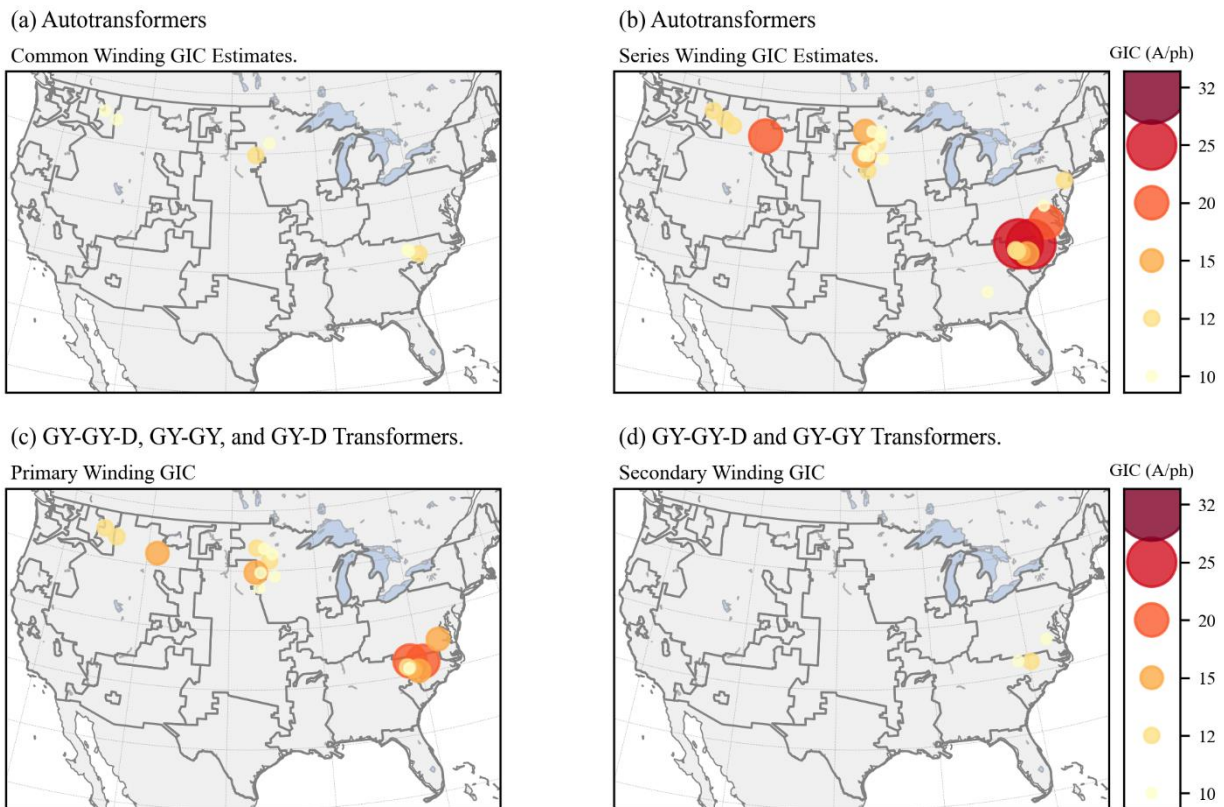


Figure 4. GIC Model outputs from the 2024 Mother's Day Gannon storm. The maximum field times were determined by applying a five-minute rolling mean to the maximum amplitudes of geoelectric field components at magnetotelluric sites, then using this smoothed data to identify peaks during the event.

We begin by reporting the GIC values for the 2024 Gannon storm, which was the largest recorded space weather event since the 2003 Halloween storm. The results are shown in Figure 4. A maximum geoelectric field of 12 V/km was recorded during the entire storm, though during the peak period when maximum amplitudes were measured across all sites, the highest value reached only 2 V/km.

During the period of maximum geoelectric magnitudes, we recorded peak GIC values of 32 A/ph. As expected, these values were predominantly observed in the serial windings of autotransformers and primaries of grounded Wye types. These peak values were most prevalent along the northern eastern coastline and in regions where maximum solid earth conductivities are noted.

Figure 5 shows the GIC outputs from the power model for the 1/100-year event scenario. The Northern Midwest region reports the highest incidences of GIC within substations, complementing previously reported magnitudes of geoelectric fields and transmission lines in literature.

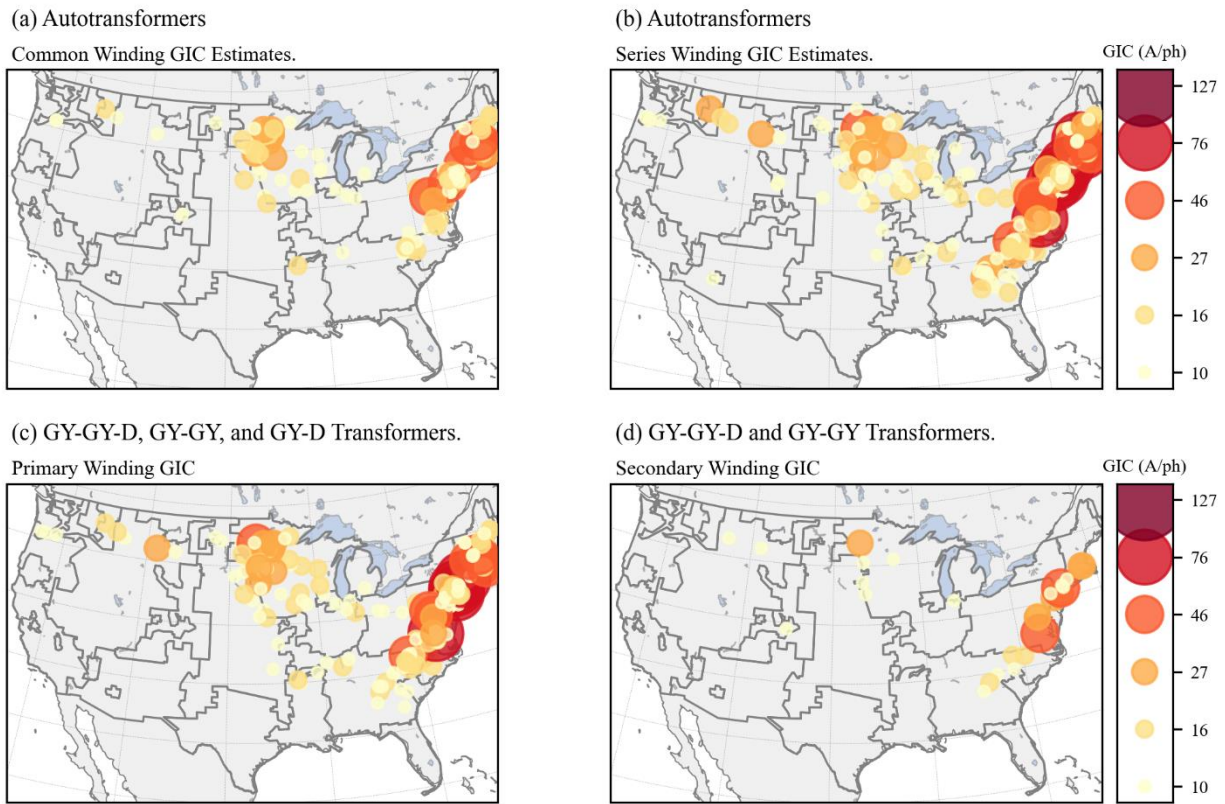


Figure 5. GIC plots from a modeled 100-year scenario by transformer type. The magnetic field data from identified storm periods within the past 39 years were interpolated with SECS to the magnetotelluric sites and convolved with site conductivity data to generate geoelectric fields. The maximum amplitudes of these fields were then fitted to a power law distribution to generate hazard maps.

For the 100-year event scenario, eleven substations recorded GIC values exceeding the NERC thermal heating withstand threshold. The primary windings of transformers experienced a maximum GIC value of 127 Amperes during this scenario. Table 1 lists the states containing the majority of affected substations.

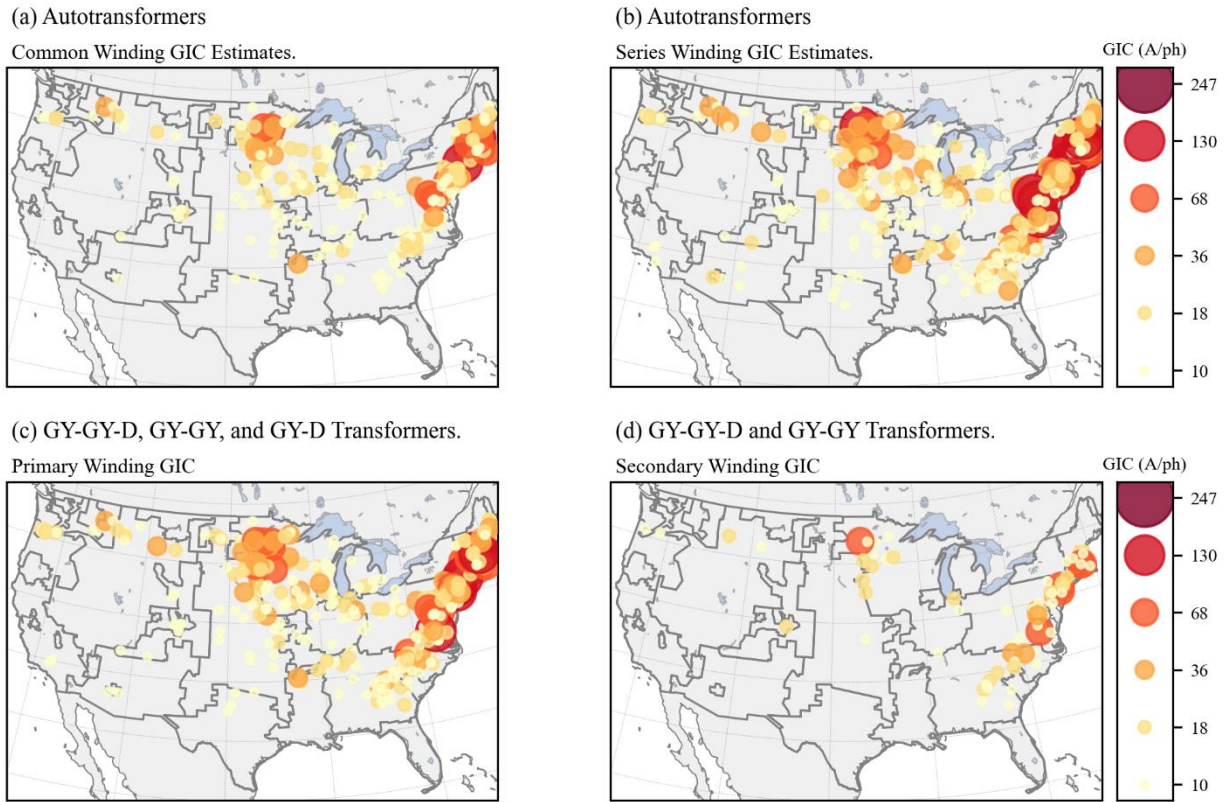


Figure 6. 500-year event GIC outputs. GIC values (A/ph) for identified transformers were derived by averaging GIC per node across all randomized examined scenarios. The method assumes substations can be ideally composed of autotransformers, three-winding or two-winding grounded Wyes.

Figure 6 and Figure 7 show respectively the GIC outputs from the 500-year and 1000-year return periods. For the 500-year event scenario, the maximum observed GIC value reached 247 A/ph. Within the modeled network architecture, the most severely affected states were, with damaged transformers in parentheses, Massachusetts (16), New Jersey (10), New Hampshire (8), Minnesota (7), Virginia (6), and Pennsylvania (6).

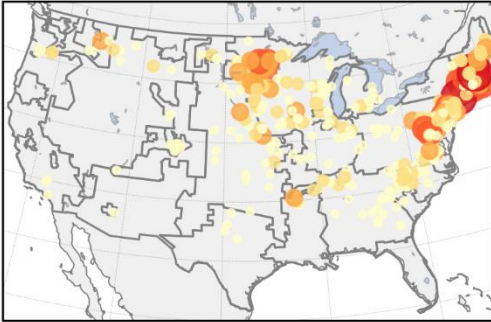
For the 1000-year event scenario, the maximum GIC value reached 320 A/ph. Many affected transformers were in New Jersey (14), Massachusetts (17), Minnesota (18), Pennsylvania (9), New Hampshire (10), Maine (3), Virginia (7), and South Dakota (8). Across all analyzed scenarios, grounded Wye-type transformers were predominantly identified as susceptible to failure.

Table 1. The number of transformers reporting GIC values above 75 A/ph (the NERC GIC withstand threshold) for each examined extreme storm event.

Return Period	Annual Probability	States (Transformer Units)
100-year event	1%	New Jersey (4), Connecticut (2), Virginia (2), Massachusetts (1), New Hampshire (1), Pennsylvania (1)
500-year event	0.2%	Massachusetts (16), New Jersey (10), New Hampshire (8), Minnesota (7), Pennsylvania (6), Virginia (6), North Carolina (3), South Dakota (3), Connecticut (2), Maryland (2), North Dakota (2), West Virginia (2), Rhode Island (1)
1000-year event	0.1%	Minnesota (18), Massachusetts (17), New Jersey (14), New Hampshire (10), Pennsylvania (9), South Dakota (8), Virginia (7), Maryland (4), Connecticut (3), Maine (3), North Carolina (3), Georgia (2), North Dakota (2), Rhode Island (2), West Virginia (2), Montana (1)

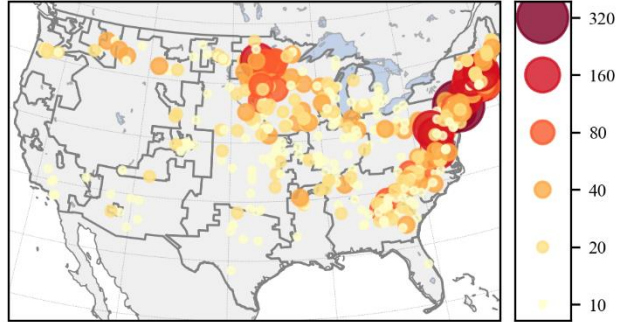
(a) Autotransformers

Common Winding GIC Estimates.



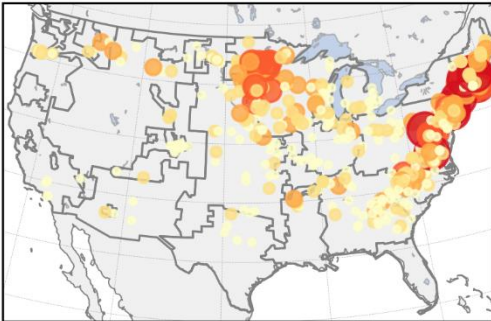
(b) Autotransformers

Series Winding GIC Estimates.



(c) GY-GY-D, GY-GY, and GY-D Transformers.

Primary Winding GIC



(d) GY-GY-D and GY-GY Transformers.

Secondary Winding GIC

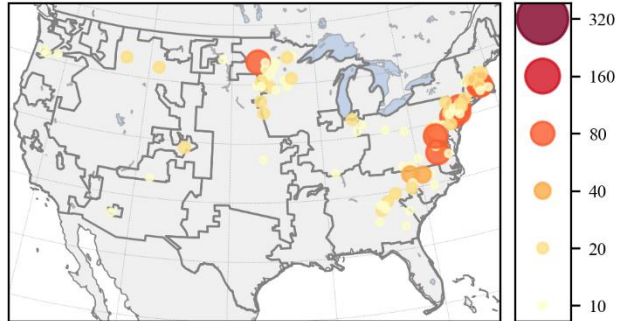


Figure 7. 1000-year event GIC outputs. GIC values (A/ph) for identified transformers were derived by averaging GIC per node across all randomized examined scenarios

4.3 What are the potential socio-economic impacts for different space weather scenarios in terms of population disruption and lost Gross Domestic Product (GDP)?

In addressing this research question, we examine the economic repercussions of transformer failures at different GIC tolerance levels. While focusing on thermal thresholds, we use these as proxies for various GIC-induced power grid instabilities. GDP impact is estimated based on the number of affected businesses per NAICS sector, using their gross output as a proxy for daily economic losses. To account for uncertainties in substation failures, a Monte Carlo simulation approach is applied to estimate the direct impacts.

The Ghosh Input-Output model is then employed to derive the indirect economic impacts, capturing the broader ripple effects across the economy. Together, the direct and indirect impacts produce the total GDP impact, which is assessed across three confidence intervals: the 2.5th percentile (most optimistic), 50th percentile (median), and 97.5th percentile (most pessimistic).

These results are presented in Figure 8, which illustrates the failed transformers, businesses impacted, and population affected across varying sensitivity thresholds and return periods. The total economic impact for these examined scenarios is shown in Figure 9. The relationship between transformer failures and GIC sensitivity thresholds reveals a clear inverse correlation: lower thresholds lead to significantly higher failure rates. At the lowest threshold of 25 A/ph, transformer failures increase sharply with return periods, surpassing 500 failures during a 1,000-year event. In contrast, higher thresholds between 100-150 A/ph demonstrate far greater resilience, with failure counts remaining low and stable even under extreme return periods.

Population impacts follow a similar trajectory, intensifying as thresholds decrease and return periods lengthen. At 25 A/ph, the affected population exceeds 40 million during a 1,000-year event, reflecting the widespread disruptions caused by cascading transformer failures. However, higher thresholds between 75-150 A/ph contain the population impact to far more manageable levels, below 20 million, underscoring the critical role of grid resilience in mitigating societal consequences.

Business disruptions mirror the population trends across different sensitivity thresholds. For a 1,000-year return period at 25 A/ph, over 1.2 million businesses experience disruption. In contrast, thresholds between 100-150 A/ph result in significantly lower (below 0.5 million) business impacts, demonstrating the system's capacity to withstand higher GIC levels with minimal economic consequences.

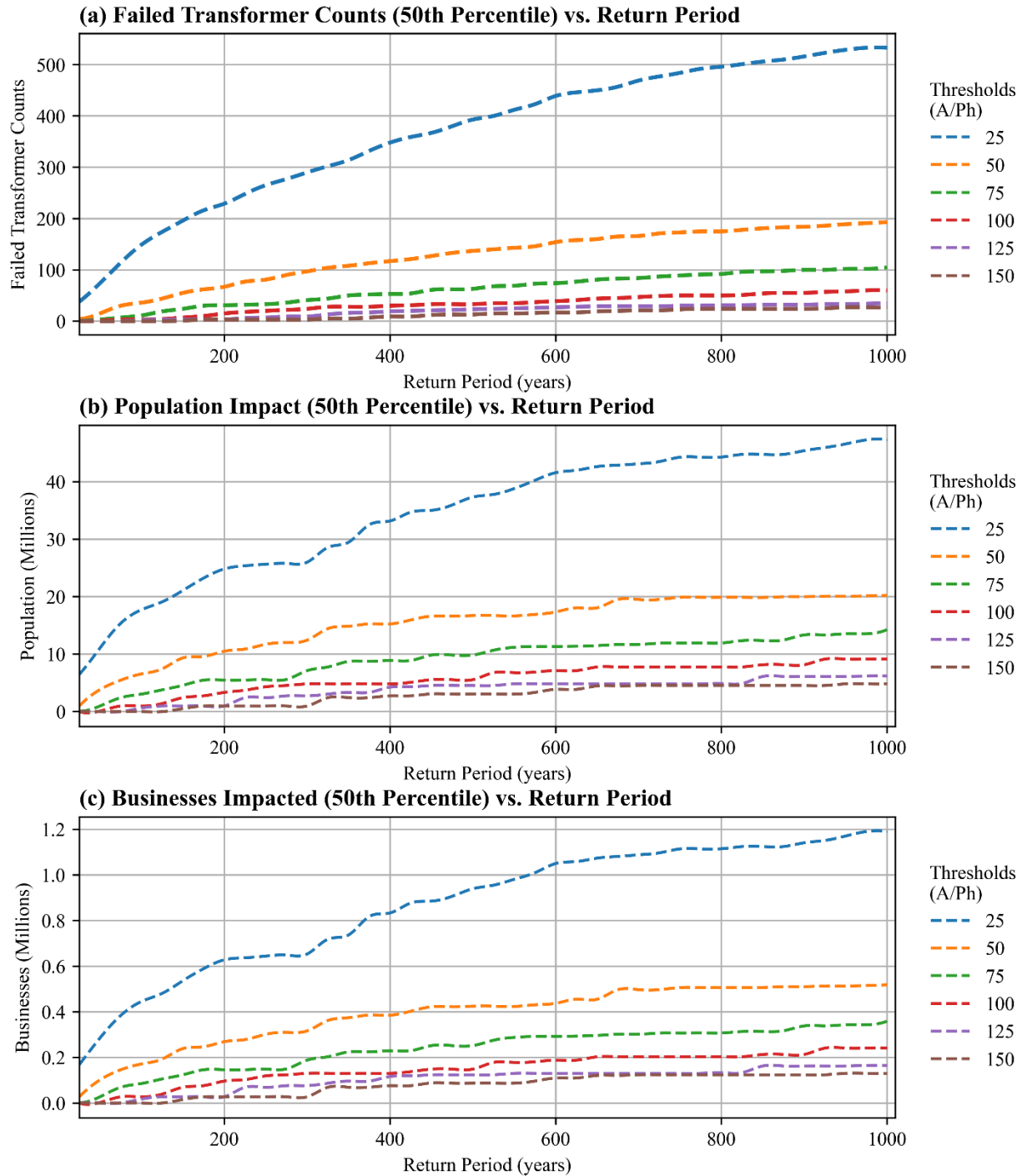


Figure 8. Asset failures and resulting population and business impacts across different sensitivity thresholds and return periods. (a) indicates the transformer failures. (b) shows the population impacted. (c) indicates the businesses affected.

Collectively, the impacts measured in transformer failures, population affected, and business disruptions are highly sensitive to the GIC threshold. Lower thresholds produce disproportionate effects, which escalate

non-linearly with longer return periods. This non-linear growth highlights the compounding nature of extreme events, where increasing severity leads to progressively greater consequences across infrastructure, society, and the economy.

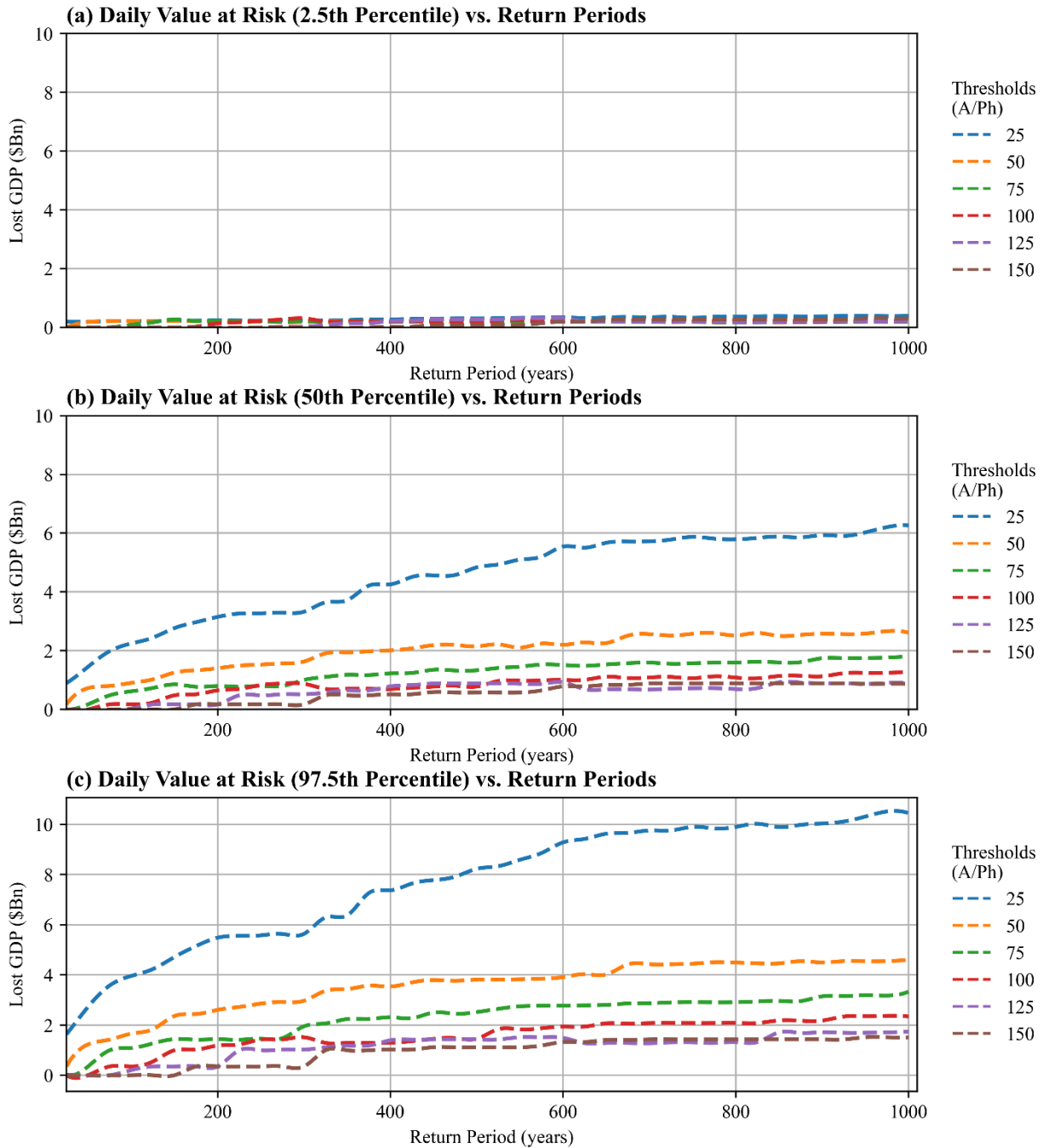


Figure 9. Total direct and indirect economic impacts for different sensitivity thresholds and return periods. (a) indicates the most optimistic bound (2.5th percentile), showing minimal GDP losses across all thresholds and return periods. (b) represents the median costs incurred (50th percentile), showing moderate economic impacts that increase with longer return periods and lower GIC thresholds. (c) illustrates the

most pessimistic bound (97.5th percentile), where severe economic disruptions occur, with GDP losses exceeding billions per day under extreme storm scenarios at lower sensitivity thresholds.

At the 2.5th percentile, GDP impact remains negligible across return periods for all sensitivity thresholds. This suggests that under optimistic failure scenarios (minimal transformer outages), the economic impact is largely contained even for extreme storm return periods. For the 50th percentile, GDP losses increase nonlinearly with decreasing GIC thresholds and higher return periods. For the lowest threshold (25 A/ph), daily GDP losses approach \$6 billion by the 1,000-year return period. Higher thresholds (e.g., 75–150 A/ph) show significantly reduced GDP losses, stabilizing below \$1 billion.

For the 97.5th percentile, under worst-case conditions, GDP losses for the 25 A/ph threshold exceed \$10 billion daily at longer return periods. Lower thresholds (e.g., 25–50 A/ph) dominate the upper-bound losses, indicating extreme sensitivity to transformer failure thresholds. For thresholds above 75 A/ph, losses remain below \$4 billion. The GDP impacts are highly sensitive to the assumed GIC threshold. Lower thresholds significantly amplify economic losses. Accordingly, economic impacts increase with return period due to the rising frequency of severe GMD events and cascading failures.

Sensitivity to GIC thresholds highlights the importance of transformer resilience and protection systems. The sharp increase in impacts at lower thresholds demonstrates how economic activity depends on grid resilience. Grid configurations, transformer protection systems, and GIC mitigation measures are critical for reducing failures and their associated societal and economic impacts.

Figure 10 presents the total sectoral breakdown of impacts by NAICS categories. The analysis is restricted to 100, 500, and 1,000-year return periods while applying a NERC thermal threshold of 75 Amperes. Since these results are derived from statistical extrapolations, the patterns observed here are consistent across other thresholds (see the appendix for additional figures).

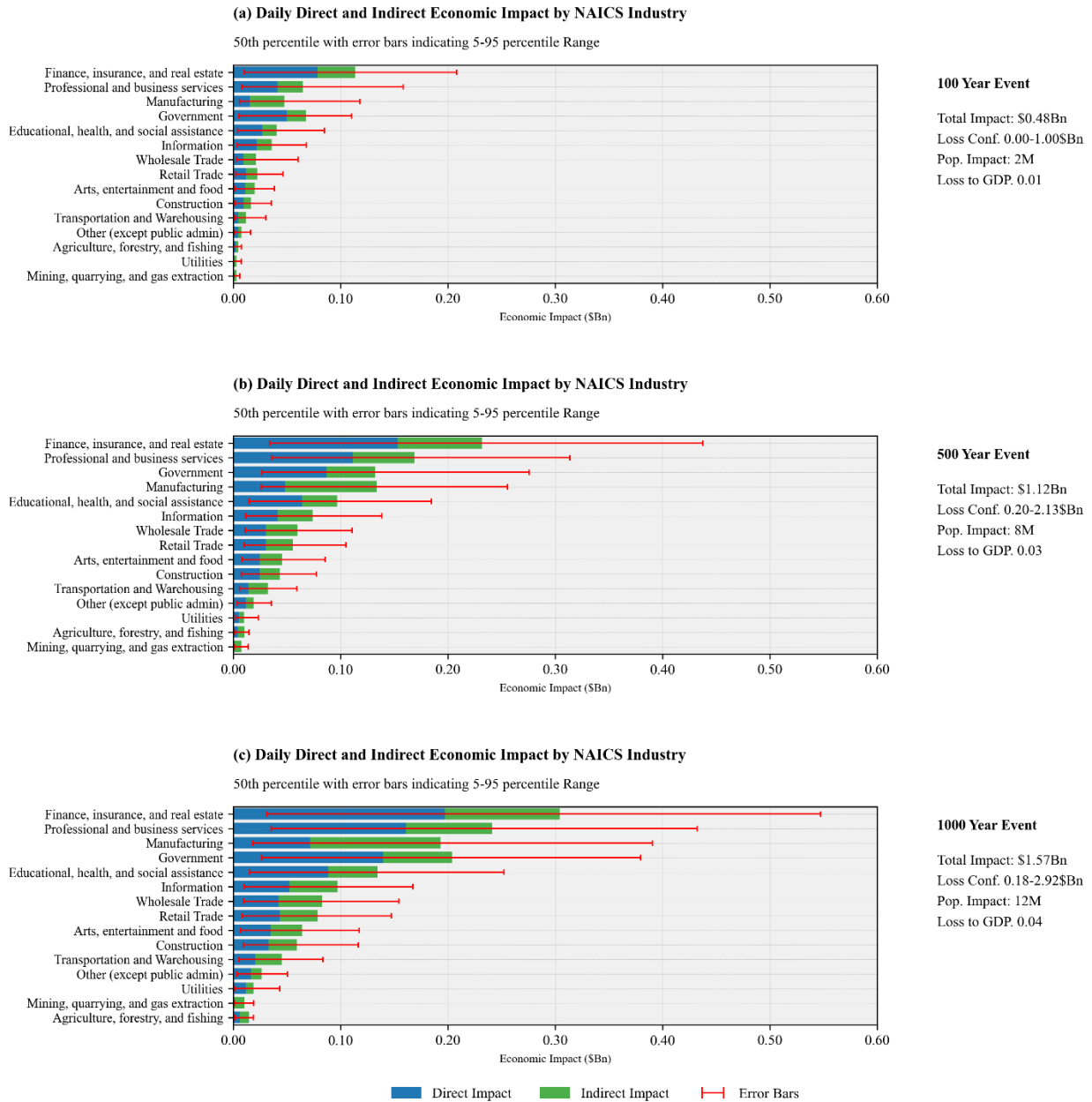


Figure 10. Industrial breakdown of direct impacts from supply chain disruptions due to space weather. For transformers recording GIC above the NERC 75A threshold, stochastic Monte Carlo simulation was used to derive the 2.5th, 50th, and 95th percentiles of direct impact within the cumulative distribution. The Ghosh model was then applied to estimate gross value-added losses across this investigated range.

We report sectorial impact for selected return periods using NERC’s conservative threshold of 75 A/Ph. For a 100-year return period, impacts remain moderate while revealing emerging vulnerabilities. The failure of 11 transformers disrupts approximately 0.09 million businesses and affects 3.05 million people. Economic losses range between \$0.09 billion (2.5th percentile) and \$1.09 billion (97.5th percentile), with a median estimate of \$0.62 billion.

Sector-specific impacts for the 100-year event show the Finance, Insurance, and Real Estate (FIRE) sector bearing the largest losses at \$0.21 billion across direct and downstream impacts. Professional and Business Services follow at \$0.16 billion, while Government, Manufacturing, and Educational Health and Social Assistance (EHSA) sectors face impacts of \$0.11 billion, \$0.12 billion, and \$0.08 billion respectively.

The 250-year event shows marked escalation, with 33 transformer failures disrupting 0.15 million businesses and affecting 5.56 million people. GDP impacts increase to between \$0.22 billion and \$1.46 billion (2.5th to 97.5th percentile), with a median of \$0.80 billion.

For a 500-year return period, impacts become substantial with 63 transformer failures affecting 0.25 million businesses and 9.84 million people. GDP losses range from \$0.20 billion to \$2.52 billion, with a median of \$1.33 billion. The most severe economic impacts are concentrated in the FIRE sector at \$0.43 billion, followed by Professional and Business Services at \$0.31 billion, while Government, Manufacturing, and EHSA services experience impacts ranging from \$0.18 billion to \$0.30 billion.

The 1,000-year event represents catastrophic impact levels, with 105 transformer failures disrupting 0.36 million businesses (approximately 3.57% of the total population) and affecting 14.27 million people. GDP losses escalate to between \$0.21 billion and \$3.33 billion, with a median of \$1.81 billion. Sectoral impacts intensify with the FIRE sector experiencing losses up to \$0.58 billion, Professional and Business Services reaching \$0.41 billion, and other key sectors including Manufacturing, Government, and EHSA services seeing impacts between \$0.25 billion and \$0.39 billion.

Analysis of higher thresholds (100, 125, and 150 A/Ph) shows significantly reduced impacts, with transformer failures, business disruptions, and population effects remaining lower, and total GDP losses rarely exceeding \$1.5 billion, contrasting with the severe impacts at 75 A/Ph. This emphasizes the critical importance of grid resilience improvements and targeted mitigation measures. Moreover, these results demonstrate the concentration of economic consequences in financial and professional services, with cascading effects across essential industries.

5. Discussion

In this section, we review the results from the method with respect to the defined research questions.

5.1 Using open-source data, what is the structure of the US electricity transmission infrastructure network?

Every power system consists of generation, transmission, and distribution networks to consumers. This study analyzes extra-high voltage transmission and distribution networks based on open data metadata classification. Although, manual verification using Google Earth imagery invalidated some classifications, identifying some substations as generation sites. This study also models a power system representation from open data to understand the grid from a geospatial perspective. Using spatial set theories, we explore grid patterns, focusing on nodes (substations) and edges (transmission lines) through geospatial intersections to identify busbars—points of connection to transformer primaries and secondaries. Our methodology identifies and categorizes substation transformer types within the grid model, including autotransformer substations and grounded Wye configurations. The Wye configurations encompass Wye-Wye, Delta-Wye (Generator Step-Up Units), and three-winding grounded Wye-Wye-Delta transformers.

The US power grid is a complex infrastructure with over a million kilometers of transmission lines and more than 50,000 substations. Theoretical modeling of this system is therefore challenging. At the highest level, the grid is divided into three regions: the Western, Eastern, and Texas (ERCOT) power pools. There is compelling evidence that scenarios involving multiple substation failures could potentially trigger complete grid failure. For example, isolated systems like the Texas grid could experience state-wide failure.

Therefore, our analysis presents the most optimistic socio-economic impact scenarios. Studies show that failure in a transmission substation can lead to cascaded failures due to power overload. Research indicates that failure in just 2% of the transmission system could lead to 60% of the system failing (Albert et al., 2004). For instance, failure of a single substation may result in a 25% loss of network capacity (Kinney et al., 2005). Studies further reveal that even small, localized failures (20%) can significantly impact the grid, causing up to 80% of failures (Ji et al., 2016). Analysis of distribution system topology indicates that most are radial, meaning node failure can cascade downstream. Our failure analysis models the power system to be comprised of a radial network topology. Unlike transmission systems, however, distribution system failures are typically localized, affecting smaller areas. Minor failures can also trigger overload cascades, especially if a substation is a hub or feeder to multiple substations. Additionally, there is a 40% chance of failure cascading downstream to dependent substations from a failed node.

5.2 How vulnerable is the US electricity transmission infrastructure network under different space weather scenarios?

We report maximum geoelectric field magnitudes that demonstrate a clear scaling with event severity: 29 V/km for 100-year events, 45 V/km for 500-year events, and 53 V/km for 1000-year events, based on the USGS approach (Love et al., 2018). Our model diverges slightly in data fitting methodology: while the USGS identifies maximum absolute geoelectric fields over entire storm periods for all examined sites, our method applies a 20-minute rolling mean, convolving geoelectric vector time series with their magnitudes to capture peak values consistently across the US. Moreover, we have reproduced hazard maps for the entire United States using impedance site data from the USGS EarthScope Array and USMT campaigns.

The geoelectric fields at the sites, derived using SECs, are interpolated onto transmission lines to compute electro-potentials, which serve as GIC voltage sources. A maximum electromotive force of 1.5 kV is recorded across scenarios. The derived potentials are fitted to a power-law distribution to extract extreme value statistics. To preserve field directionality, the maximum absolute values are first extracted, their original signs retained, and the signed values are appended back to the extrapolated potentials after fitting. This approach ensures accurate modeling of current injection directionality into substations. Using assumptions from the Horton grid, we estimate current injections from these scalar potentials (Horton et al., 2012). While slight variations in grid-specific resistance (e.g., due to temperature fluctuations) are noted, they do not significantly skew the results.

The Gannon storm analysis provides real-world comparison, where a maximum field of 12 V/km over the entire storm duration was observed, though peak period measurements reached only 2 V/km. During the periods of maximum geoelectric magnitude, peak GIC values of 32 A/ph were observed, predominantly in autotransformer serial windings and grounded Wye-type transformer primaries. Geographic trends emerged clearly in our analysis, with field intensities and induced voltage sources diminishing southward, while the Northern Midwest region exhibited the highest GIC concentrations within substations, aligning with previous literature on regional geoelectric characteristics. Maximum GIC values are also recorded in these hazard zones, suggesting these areas may benefit from GIC mitigating devices.

This study is useful for analyzing power system resilience. Power system resilience reflects the system's capacity to withstand external hazards and recovery. By identifying substations with peak field magnitudes, we conducted a comprehensive resilience assessment. While rare, GICs can lead to thermal heating, causing transformer failures that may persist for weeks or months impacting millions of consumers. Standard mitigation measures, such as series compensators and neutral point blocking devices, are typically implemented to reduce GIC effects. Our study models nodes and transmission lines, applying uncertainty quantification in failure analysis. While we exclude protective devices in our model, we assign system failure probabilities to establish confidence intervals, ranging from optimistic (no failure) to pessimistic (total collapse), providing a comprehensive view of resilience in terms of potential system response.

5.3 What are the potential socio-economic impacts for different space weather scenarios in terms population disruption and lost GDP?

Our analysis adopts a comprehensive approach to assessing space weather hazards' economic implications, employing the Ghosh Input-Output model to capture both direct and sectorial-interdependence impacts. The relationship between transformer failures and GIC sensitivity thresholds reveals that at lower thresholds (25 A/ph), failures increase dramatically with longer return periods, exceeding 500 failures during 1,000-year events, while higher thresholds (100-150 A/ph) maintain stable, low failure counts even under extreme conditions.

For space weather extreme value scenarios leading to thermal heating voltage collapse, total daily economic impacts vary significantly across confidence intervals. At the 50th percentile, GDP losses increase nonlinearly with decreasing GIC thresholds and higher return periods, approaching \$6 billion daily for the lowest threshold (25 A/ph) during 1,000-year events. Under the 97.5th percentile worst-case conditions, GDP losses can exceed \$10 billion daily at longer return periods for the 25 A/ph threshold, while thresholds above 75 A/ph contain losses below \$4 billion.

Using a conservative threshold of 75 A/Ph, sectoral analysis reveals that the FIRE sector experiences the most significant combined direct and indirect impacts, reaching \$0.58 billion in a 1,000-year event scenario, due to its heavy dependence on downstream sectors. Manufacturing emerges as another severely affected sector, facing impacts of up to \$0.39 billion in extreme scenarios, due to its strong backward and forward linkages across industries, followed by EHSA and Professional and Business Services, which face impacts of \$0.25 billion and \$0.41 billion respectively in 1,000-year events. Even in more moderate 100-year scenarios, FIRE sector losses reach \$0.21 billion, while Professional and Business Services face \$0.16 billion in losses, and Manufacturing, Government, and EHSA sectors experience impacts ranging from \$0.08 billion to \$0.12 billion. In contrast, sectors primarily selling final products, such as agriculture, forestry, fishing, and hunting; mining, quarrying, and oil and gas extraction; and transportation and warehousing, show greater resilience due to limited forward linkages. The magnitude of indirect shock in each sector depends critically on its interconnectedness within the broader economic network, emphasizing the importance of considering both direct infrastructure vulnerabilities and cascading economic effects in resilience planning.

In this section we also highlight economic model limitations in estimating direct and indirect losses. First is that we are limited by the lack of more granular regional economic data. For example, the regional GDP is acquired based on the estimates of business proportions by NAICS code. This means that individual establishments by NAICS code contribute equally to the total gross value added by that sector.

Secondly, we hypothesize that consumers and businesses depend entirely on electricity from the regional grid in production and other economic activities. This is generally true for households; however, many enterprises have power redundancies substituting services usually provided by electricity networks. For example, data centers and enterprises providing essential services ensure the high availability of their goods and services by investing in alternate power sources. As much as they might incur extra costs, they would not experience a total loss of productivity.

Thirdly, it is likely that businesses and consumers will compensate for the lost productivity in the future. In other words, a loss of power for a particular duration may necessitate businesses to replenish lost productivity by working extra hours or hiring more employees. Consequently, while the impact will temporarily take a toll on consumers and businesses, recovery for the loss of productivity may be anticipated.

Finally, there is a notable concern about the plausibility of the Ghosh supply-side model in estimating supply chain impacts. The theoretical underpinning of this model is that increased industrial output will stimulate demand from the downstream industries, contrary to Leontief's upstream economic impact. The input-output models also assume a linear inter-industry economic dependency. This oversimplification overlooks complex non-linear dynamics of actual economies.

6. Conclusion

This work presents a novel approach to estimating the economic impact of electricity transmission infrastructure failure due to space weather. Our methodology couples existing geophysical and GIC estimation models with new Continental United States power grid geospatial model to assess potential GIC impacts across different space weather scenarios.

Using this coupled modeling framework, we analyzed the May 2024 Gannon storm, which recorded maximum GIC values of 32 amperes per phase (A/ph). Extreme event statistics reveal a predictable scaling of geoelectric field magnitudes with event severity, with maximum geoelectric potentials on high-voltage transmission lines reaching up to 1.5 kilovolts. Transformer failures escalate exponentially at lower GIC thresholds (e.g., 25 A/ph), with over 500 failures predicted during 1,000-year return periods, presenting disproportionate risks to isolated systems such as the Texas (ERCOT) grid.

From an economic perspective, the cascading effects of these failures extend far beyond direct infrastructure damage. Daily GDP losses range from \$6 billion to over \$10 billion during extreme events, with sectors such as FIRE, Manufacturing, and Professional Services experiencing the greatest impacts due to their interconnected roles within the broader economic network. Even under more conservative thresholds (75 A/ph) aligned with NERC thermal withstand limits, significant economic disruptions are observed.

Despite the robust insights provided, there are gaps in our research methodology that future studies could address. Key parameters missing from our power system model include line resistances, transformer types, GIC blocking devices, and specific transformer specifications. While Monte Carlo simulations applied to these parameters used values from the Horton grid, more precise data would enhance accuracy. Our vulnerability assessment focuses exclusively on thermal effects in transformers, serving as a starting point for understanding GIC impacts. Future research should expand this scope to consider voltage instability and harmonic distortions. Additionally, while our economic modeling employs a static Ghosh model to capture sectoral interdependencies, the use of more dynamic approaches such as Computable General

Equilibrium (CGE) models could improve the representation of sectoral economic relationships. These findings are crucial for industry stakeholders, insurers, policymakers, and infrastructure planners aiming to develop compensation mechanisms, formulate effective policy responses, and enhance resilience against space weather hazards.

Acknowledgments

This material is based upon work supported by the NSF National Center for Atmospheric Research, which is a major facility sponsored by the US National Science Foundation under Cooperative Agreement No. 1852977. The project upon which this article is based was funded through the NSF NCAR Early-Career Faculty Innovator Program under the same Cooperative Agreement. We also gratefully acknowledge funding from the ChronoStorm NSF RAPID grant (#2434136), co-funded by the GEO/AGS Space Weather Research and the ENG/CMMI Humans, Disasters, and the Built Environment programs.

Open Research

Python and R languages are used for data collection, exploration, and analytics. The project data collection, analysis, and visualizations are available and hosted on GitHub (Bor, 2024a). A zipped file of the raw data files used in scenario modeling is accessible from Zenodo (Bor, 2024b).

References

- Abda, Z.M.K., Aziz, N.F.A., Kadir, M.Z.A.A., Rhazali, Z.A., 2020. A Review of Geomagnetically Induced Current Effects on Electrical Power System: Principles and Theory. *IEEE Access* 8, 200237–200258. <https://doi.org/10.1109/ACCESS.2020.3034347>
- Albert, D., Halbedl, T., Renner, H., Bailey, R.L., Achleitner, G., 2019. Geomagnetically induced currents and space weather - A review of current and future research in Austria, in: 2019 54th International Universities Power Engineering Conference (UPEC). Presented at the 2019 54th International Universities Power Engineering Conference (UPEC), pp. 1–6. <https://doi.org/10.1109/UPEC.2019.8893515>
- Albert, R., Albert, I., Nakarado, G.L., 2004. Structural vulnerability of the North American power grid. *Phys. Rev. E* 69, 025103. <https://doi.org/10.1103/PhysRevE.69.025103>
- Banerjee, A., Bej, A., Chatterjee, T.N., 2012. On the existence of a long range correlation in the Geomagnetic Disturbance storm time (Dst) index. *Astrophys. Space Sci.* 337, 23–32. <https://doi.org/10.1007/s10509-011-0836-1>
- Baum, S.D., 2023. Assessing natural global catastrophic risks. *Nat. Hazards* 115, 2699–2719. <https://doi.org/10.1007/s11069-022-05660-w>
- BEA, 2023a. BEA Interactive Data Application [WWW Document]. URL <https://tinyurl.com/4busxa7y> (accessed 3.4.24).
- BEA, 2023b. Input-Output Accounts Data | U.S. Bureau of Economic Analysis (BEA) [WWW Document]. URL <https://www.bea.gov/industry/input-output-accounts-data> (accessed 3.4.24).
- Bhowmik, P., Yeates, A.R., Rice, O.E.K., 2022. Exploring the Origin of Stealth Coronal Mass Ejections with Magnetofrictional Simulations. *Sol. Phys.* 297, 41. <https://doi.org/10.1007/s11207-022-01974-x>
- Bor, D., 2024a. SPWIO [WWW Document]. GitHub. URL <https://github.com/denniesbor/spwio> (accessed 12.22.24).
- Bor, D., 2024b. Geomag data. <https://doi.org/10.5281/zenodo.14231083>
- Boteler, D.H., Pirjola, R.J., 2017. Modeling geomagnetically induced currents. *Space Weather* 15, 258–276. <https://doi.org/10.1002/2016SW001499>
- Botezatu, U.-E., 2023. Attempted cyber security of systems and operations in outer space: an overview of space-based vulnerabilities. *Romanian Cyber Secur. J.* 5, 67–76.
- Botzen, W.J.W., Deschenes, O., Sanders, M., 2019. The Economic Impacts of Natural Disasters: A Review of Models and Empirical Studies. *Rev. Environ. Econ. Policy* 13, 167–188. <https://doi.org/10.1093/reep/rez004>
- Bureau, U.C., 2023. Statistics of U.S. Businesses [WWW Document]. Census.gov. URL <https://www.census.gov/programs-surveys/susb.html> (accessed 2.12.24).
- Bureau, U.C., 2020. 2020 Population and Housing State Data [WWW Document]. Census.gov. URL <https://www.census.gov/library/visualizations/interactive/2020-population-and-housing-state-data.html> (accessed 3.4.24).
- Cander, L.R., 2019. *Ionospheric Space Weather*, Springer Geophysics. Springer International Publishing, Cham. <https://doi.org/10.1007/978-3-319-99331-7>
- Cantelmo, A., Melina, G., Papageorgiou, C., 2023. Macroeconomic outcomes in disaster-prone countries. *J. Dev. Econ.* 161, 103037. <https://doi.org/10.1016/j.jdeveco.2022.103037>
- Chen, P., Scown, C., Matthews, H.S., Garrett, J.H., Hendrickson, C., 2009. Managing Critical Infrastructure Interdependence through Economic Input-Output Methods. *J. Infrastruct. Syst.* 15, 200–210. [https://doi.org/10.1061/\(ASCE\)1076-0342\(2009\)15:3\(200\)](https://doi.org/10.1061/(ASCE)1076-0342(2009)15:3(200))
- Chopra, S.S., Khanna, V., 2015. Interconnectedness and interdependencies of critical infrastructures in the US economy: Implications for resilience. *Phys. Stat. Mech. Its Appl.* 436, 865–877. <https://doi.org/10.1016/j.physa.2015.05.091>

- CISA, 2024. Critical Infrastructure Sectors | CISA [WWW Document]. URL <https://www.cisa.gov/topics/critical-infrastructure-security-and-resilience/critical-infrastructure-sectors> (accessed 1.28.24).
- de Santana Ribeiro, L.C., Pereira, E.J. de A.L., Perobelli, F.S., Pereira, H.B. de B., 2023. Sectoral Interdependence, Network Analysis, and Regional Resilience in Brazil. *Lat. Am. Bus. Rev.* 24, 177–205. <https://doi.org/10.1080/10978526.2022.2074441>
- Deng, Y., Song, L., Zhou, J., Xu, N., Ni, G., Wang, L., 2020. Analysis of Failures and Influence Factors of Critical Infrastructures: A Case of Metro. *Adv. Civ. Eng.* 2020, e2301276. <https://doi.org/10.1155/2020/2301276>
- Dickinson, T.L., Gannon, J.L., 2023. SWAG Recommendations Call For Strategic and New Activities Across the Space Weather Enterprise.
- Dimmock, A.P., Rosenqvist, L., Hall, J.-O., Viljanen, A., Yordanova, E., Honkonen, I., André, M., Sjöberg, E.C., 2019. The GIC and Geomagnetic Response Over Fennoscandia to the 7–8 September 2017 Geomagnetic Storm. *Space Weather* 17, 989–1010. <https://doi.org/10.1029/2018SW002132>
- Eastwood, J.P., Biffis, E., Hapgood, M.A., Green, L., Bisi, M.M., Bentley, R.D., Wicks, R., McKinnell, L.-A., Gibbs, M., Burnett, C., 2017. The Economic Impact of Space Weather: Where Do We Stand? *Risk Anal.* 37, 206–218. <https://doi.org/10.1111/risa.12765>
- Facsco, G., Koban, G., Biro, N., Lkhagvadorj, M., 2023. Space Weather Effects on Critical Infrastructure. <https://doi.org/10.48550/arXiv.2306.16380>
- Firoz, K.A., Cho, K.-S., Hwang, J., Phani Kumar, D.V., Lee, J.J., Oh, S.Y., Kaushik, S.C., Kudela, K., Rybanský, M., Dorman, L.I., 2010. Characteristics of ground-level enhancement–associated solar flares, coronal mass ejections, and solar energetic particles. *J. Geophys. Res. Space Phys.* 115. <https://doi.org/10.1029/2009JA015023>
- Forbes, K.F., St. Cyr, O.C., 2004. Space weather and the electricity market: An initial assessment. *Space Weather* 2. <https://doi.org/10.1029/2003SW000005>
- Galbusera, L., Giannopoulos, G., 2018. On input-output economic models in disaster impact assessment. *Int. J. Disaster Risk Reduct., Understanding and mitigating cascading crises in the global interconnected system* 30, 186–198. <https://doi.org/10.1016/j.ijdr.2018.04.030>
- Ganushkina, N.Yu., Liemohn, M.W., Dubyagin, S., 2018. Current Systems in the Earth’s Magnetosphere. *Rev. Geophys.* 56, 309–332. <https://doi.org/10.1002/2017RG000590>
- Gopalswamy, N., 2022. The Sun and Space Weather. *Atmosphere* 13, 1781. <https://doi.org/10.3390/atmos13111781>
- Gopalswamy, N., 2016. History and development of coronal mass ejections as a key player in solar terrestrial relationship. *Geosci. Lett.* 3, 8. <https://doi.org/10.1186/s40562-016-0039-2>
- Gritsutenko, S., Korovkin, N., Sakharov, Y., Sokolova, O., 2023. Assessment of Geomagnetically Induced Currents Impact on Power Grid Modelling. *Magnetism* 3, 135–147. <https://doi.org/10.3390/magnetism3020011>
- Hajra, R., 2022. Intense Geomagnetically Induced Currents (GICs): Association with Solar and Geomagnetic Activities. *Sol. Phys.* 297, 14. <https://doi.org/10.1007/s11207-021-01945-8>
- Hall, J.W., Thacker, S., Ives, M.C., Cao, Y., Chaudry, M., Blainey, S.P., Oughton, E.J., 2017. Strategic analysis of the future of national infrastructure. *Proc. Inst. Civ. Eng. - Civ. Eng.* 170, 39–47. <https://doi.org/10.1680/jcien.16.00018>
- Hasan, S., Foliente, G., 2015. Modeling infrastructure system interdependencies and socioeconomic impacts of failure in extreme events: emerging R&D challenges. *Nat. Hazards* 78, 2143–2168. <https://doi.org/10.1007/s11069-015-1814-7>
- Heyns, M.J., Gaunt, C.T., Lotz, S.I., Cilliers, P.J., 2020. Data driven transfer functions and transmission network parameters for GIC modelling. *Electr. Power Syst. Res.* 188, 106546. <https://doi.org/10.1016/j.epsr.2020.106546>
- Heyns, M.J., Lotz, S.I., Gaunt, C.T., 2021. Geomagnetic Pulsations Driving Geomagnetically Induced Currents. *Space Weather* 19, e2020SW002557. <https://doi.org/10.1029/2020SW002557>

- HIFLD, 2023. Transmission Lines [WWW Document]. URL <https://hifld-geoplatform.opendata.arcgis.com/datasets/geoplatform::transmission-lines/about> (accessed 11.8.23).
- Horton, R., Boteler, D., Overbye, T.J., Pirjola, R., Dugan, R.C., 2012. A Test Case for the Calculation of Geomagnetically Induced Currents. *IEEE Trans. Power Deliv.* 27, 2368–2373. <https://doi.org/10.1109/TPWRD.2012.2206407>
- Hossain, N.U.I., Amrani, S.E., Jaradat, R., Marufuzzaman, M., Buchanan, R., Rinaudo, C., Hamilton, M., 2020. Modeling and assessing interdependencies between critical infrastructures using Bayesian network: A case study of inland waterway port and surrounding supply chain network. *Reliab. Eng. Syst. Saf.* 198, 106898. <https://doi.org/10.1016/j.ress.2020.106898>
- Huang, R., Malik, A., Lenzen, M., Jin, Y., Wang, Y., Faturay, F., Zhu, Z., 2022. Supply-chain impacts of Sichuan earthquake: a case study using disaster input–output analysis. *Nat. Hazards* 110, 2227–2248. <https://doi.org/10.1007/s11069-021-05034-8>
- Hughes, J., Mcgranaghan, R., Kellerman, A.C., Bortnik, J., Arrit, R.F., Venkataramani, K., Perry, C.H., McCormick, J., Ngwira, C.M., Cohen, M., 2022. Revealing Novel Connections Between Space Weather and the Power Grid: Network Analysis of Ground-Based Magnetometer and Geomagnetically Induced Currents (GIC) Measurements. *Space Weather* 20, e2021SW002727. <https://doi.org/10.1029/2021SW002727>
- Ishii, M., Shiota, D., Tao, C., Ebihara, Y., Fujiwara, H., Ishii, T., Ichimoto, K., Kataoka, R., Koga, K., Kubo, Y., Kusano, K., Miyoshi, Y., Nagatsuma, T., Nakamizo, A., Nakamura, M., Nishioka, M., Saito, S., Sato, T., Tsugawa, T., Yoden, S., 2021. Space weather benchmarks on Japanese society. *Earth Planets Space* 73, 108. <https://doi.org/10.1186/s40623-021-01420-5>
- Ji, C., Wei, Y., Mei, H., Calzada, J., Carey, M., Church, S., Hayes, T., Nugent, B., Stella, G., Wallace, M., White, J., Wilcox, R., 2016. Large-scale data analysis of power grid resilience across multiple US service regions. *Nat. Energy* 1, 1–8. <https://doi.org/10.1038/nenergy.2016.52>
- Jonkeren, O., Giannopoulos, G., 2014. Analysing Critical Infrastructure Failure with a Resilience Inoperability Input–Output Model. *Econ. Syst. Res.* 26, 39–59. <https://doi.org/10.1080/09535314.2013.872604>
- Kataoka, R., Ngwira, C., 2016. Extreme geomagnetically induced currents. *Prog. Earth Planet. Sci.* 3, 23. <https://doi.org/10.1186/s40645-016-0101-x>
- Kelbert, A., 2023. EM Transfer Function Product Query [WWW Document]. URL <https://ds.iris.edu/spud/emtf> (accessed 4.26.24).
- Kelbert, A., 2020. The Role of Global/Regional Earth Conductivity Models in Natural Geomagnetic Hazard Mitigation. *Surv. Geophys.* 41, 115–166. <https://doi.org/10.1007/s10712-019-09579-z>
- Kelly, S., 2015a. Estimating economic loss from cascading infrastructure failure: a perspective on modelling interdependency. *Infrastruct. Complex.* 2, 7. <https://doi.org/10.1186/s40551-015-0010-y>
- Kelly, S., 2015b. Estimating economic loss from cascading infrastructure failure: a perspective on modelling interdependency. *Infrastruct. Complex.* 2, 7. <https://doi.org/10.1186/s40551-015-0010-y>
- Kerridge, D., 2001. INTERMAGNET: worldwide near-real-time geomagnetic observatory data.
- Kilpua, E., Koskinen, H.E.J., Pulkkinen, T.I., 2017. Coronal mass ejections and their sheath regions in interplanetary space. *Living Rev. Sol. Phys.* 14, 5. <https://doi.org/10.1007/s41116-017-0009-6>
- Kinney, R., Crucitti, P., Albert, R., Latora, V., 2005. Modeling cascading failures in the North American power grid. *Eur. Phys. J. B - Condens. Matter Complex Syst.* 46, 101–107. <https://doi.org/10.1140/epjb/e2005-00237-9>
- Klauber, C., Shetye, K., Overbye, T.J., Davis, K., 2020. A GIC Estimator for Electric Grid Monitoring During Geomagnetic Disturbances. *IEEE Trans. Power Syst.* 35, 4847–4855. <https://doi.org/10.1109/TPWRS.2020.3000746>

- Koks, E., Pant, R., Thacker, S., Hall, J.W., 2019. Understanding Business Disruption and Economic Losses Due to Electricity Failures and Flooding. *Int. J. Disaster Risk Sci.* 10, 421–438. <https://doi.org/10.1007/s13753-019-00236-y>
- Kolarski, A., Veselinović, N., Srećković, V.A., Mijić, Z., Savić, M., Dragić, A., 2023. Impacts of Extreme Space Weather Events on September 6th, 2017 on Ionosphere and Primary Cosmic Rays. *Remote Sens.* 15, 1403. <https://doi.org/10.3390/rs15051403>
- Kyoto, W., 2024. Plot and data output of the Dst and AE indices (Hourly Values) [WWW Document]. URL <https://wdc.kugi.kyoto-u.ac.jp/dstae/index.html> (accessed 12.23.24).
- Lin, J., Tai, K., Tiong, R.L.K., Sim, M.S., 2017. Analyzing Impact on Critical Infrastructure Using Input-Output Interdependency Model: Case Studies. *ASCE-ASME J. Risk Uncertain. Eng. Syst. Part Civ. Eng.* 3, 04017016. <https://doi.org/10.1061/AJRUA6.0000919>
- Love, J.J., Lucas, G.M., Kelbert, A., Bedrosian, P.A., 2018. Geoelectric Hazard Maps for the Mid-Atlantic United States: 100 Year Extreme Values and the 1989 Magnetic Storm. *Geophys. Res. Lett.* 45, 5–14. <https://doi.org/10.1002/2017GL076042>
- Lucas, G., Erigler-USGS, 2023. [greglucas/bezpy: REL: v0.1.1. https://doi.org/10.5281/zenodo.8395357](https://doi.org/10.5281/zenodo.8395357)
- Lucas, G.M., Love, J.J., Kelbert, A., Bedrosian, P.A., Rigler, E.J., 2020. A 100-year Geoelectric Hazard Analysis for the U.S. High-Voltage Power Grid. *Space Weather* 18, e2019SW002329. <https://doi.org/10.1029/2019SW002329>
- Luntama, J.-P., others, 2017. Report on the ESA Space-Weather Socio-Economic Study, in: *Space Weather Manager ESA SSA Programme Office, Space Weather Workshop.* pp. 2–5.
- Lyu, Y., Xiang, Y., Wang, D., 2023. Evaluating Indirect Economic Losses from Flooding Using Input–Output Analysis: An Application to China’s Jiangxi Province. *Int. J. Environ. Res. Public Health* 20, 4509. <https://doi.org/10.3390/ijerph20054509>
- MacAlester, M.H., Murtagh, W., 2014. Extreme Space Weather Impact: An Emergency Management Perspective. *Space Weather* 12, 530–537. <https://doi.org/10.1002/2014SW001095>
- Mandea, M., Chambodut, A., 2020. Geomagnetic Field Processes and Their Implications for Space Weather. *Surv. Geophys.* 41, 1611–1627. <https://doi.org/10.1007/s10712-020-09598-1>
- Matzka, J., Bronkalla, O., Tornow, K., Elger, K., Stolle, C., 2021. Geomagnetic Kp index. <https://doi.org/10.5880/KP.0001>
- Miteva, R., Samwel, S.W., Tkatchova, S., 2023. Space Weather Effects on Satellites. *Astronomy* 2, 165–179. <https://doi.org/10.3390/astronomy2030012>
- NERC, 2017. Transmission System Planned Performance for Geomagnetic Disturbance Events.
- Ngwira, C.M., Pulkkinen, A.A., 2019. An Introduction to Geomagnetically Induced Currents, in: *Geomagnetically Induced Currents from the Sun to the Power Grid.* American Geophysical Union (AGU), pp. 1–13. <https://doi.org/10.1002/9781119434412.ch1>
- NOAA, 2024. Space Weather Phenomena | NOAA / NWS Space Weather Prediction Center [WWW Document]. URL <https://www.swpc.noaa.gov/phenomena> (accessed 1.27.24).
- NOAA, 2023. Space Weather Scales | NOAA / NWS Space Weather Prediction Center [WWW Document]. URL <https://www.swpc.noaa.gov/noaa-scales-explanation> (accessed 10.24.23).
- Nowakowski, M., Dudek, E., Rosiński, A., 2023. The Influence of Varying Atmospheric and Space Weather Conditions on the Accuracy of Position Determination. *Sensors* 23, 2814. <https://doi.org/10.3390/s23052814>
- NRCAN, 2024. Magnetic Data [WWW Document]. URL <https://geomag.nrcan.gc.ca/data-donnee/sd-en.php> (accessed 12.23.24).
- Oliveira, D.M., Ngwira, C.M., 2017. Geomagnetically Induced Currents: Principles. *Braz. J. Phys.* 47, 552–560. <https://doi.org/10.1007/s13538-017-0523-y>
- Oosterhaven, J., 1988. On the plausibility of the supply-driven input-output model. *J. Reg. Sci.* 28, 203–217. <https://doi.org/10.1111/j.1467-9787.1988.tb01208.x>
- Oughton, E.J., 2024. A reproducible method for mapping electricity transmission infrastructure for space weather risk assessment.

- Oughton, E.J., 2021. The Economic Impact of Critical National Infrastructure Failure Due to Space Weather. <https://doi.org/10.48550/arXiv.2106.08945>
- Oughton, E.J., Hapgood, M., Richardson, G.S., Beggan, C.D., Thomson, A.W.P., Gibbs, M., Burnett, C., Gaunt, C.T., Trichas, M., Dada, R., Horne, R.B., 2019. A Risk Assessment Framework for the Socioeconomic Impacts of Electricity Transmission Infrastructure Failure Due to Space Weather: An Application to the United Kingdom. *Risk Anal.* 39, 1022–1043. <https://doi.org/10.1111/risa.13229>
- Oughton, E.J., Skelton, A., Horne, R.B., Thomson, A.W.P., Gaunt, C.T., 2017. Quantifying the daily economic impact of extreme space weather due to failure in electricity transmission infrastructure. *Space Weather* 15, 65–83. <https://doi.org/10.1002/2016SW001491>
- Oughton, E.J., Usher, W., Tyler, P., Hall, J.W., 2018. Infrastructure as a Complex Adaptive System. *Complexity* 2018, 3427826. <https://doi.org/10.1155/2018/3427826>
- Pamucar, D., Sarkar, B.D., Shardeo, V., Soni, T.K., Dwivedi, A., 2023. An integrated interval programming and input–output knowledge model for risk and resiliency management. *Decis. Anal. J.* 9, 100317. <https://doi.org/10.1016/j.dajour.2023.100317>
- Piersanti, M., Di Matteo, S., Carter, B.A., Currie, J., D’Angelo, G., 2019. Geoelectric Field Evaluation During the September 2017 Geomagnetic Storm: MA.I.GIC. *Model. Space Weather* 17, 1241–1256. <https://doi.org/10.1029/2019SW002202>
- Pirjola, R.J., Boteler, D.H., Tuck, L., Marsal, S., 2022. The Lehtinen–Pirjola method modified for efficient modelling of geomagnetically induced currents in multiple voltage levels of a power network. *Ann. Geophys.* 40, 205–215. <https://doi.org/10.5194/angeo-40-205-2022>
- Pulkkinen, A., Bernabeu, E., Thomson, A., Viljanen, A., Pirjola, R., Boteler, D., Eichner, J., Cilliers, P.J., Welling, D., Savani, N.P., Weigel, R.S., Love, J.J., Balch, C., Ngwira, C.M., Crowley, G., Schultz, A., Kataoka, R., Anderson, B., Fugate, D., Simpson, J.J., MacAlester, M., 2017. Geomagnetically induced currents: Science, engineering, and applications readiness. *Space Weather* 15, 828–856. <https://doi.org/10.1002/2016SW001501>
- Rajput, V.N., Boteler, D.H., Rana, N., Saiyed, M., Anjana, S., Shah, M., 2021. Insight into impact of geomagnetically induced currents on power systems: Overview, challenges and mitigation. *Electr. Power Syst. Res.* 192, 106927. <https://doi.org/10.1016/j.epsr.2020.106927>
- Rigler, E.J., Fiori, R.A.D., Pulkkinen, A.A., Wiltberger, M., Balch, C., 2019. Interpolating Geomagnetic Observations, in: *Geomagnetically Induced Currents from the Sun to the Power Grid*. American Geophysical Union (AGU), pp. 15–41. <https://doi.org/10.1002/9781119434412.ch2>
- Riley, P., Baker, D., Liu, Y.D., Verronen, P., Singer, H., Güdel, M., 2017. Extreme Space Weather Events: From Cradle to Grave. *Space Sci. Rev.* 214, 21. <https://doi.org/10.1007/s11214-017-0456-3>
- Rocchetta, R., 2022. Enhancing the resilience of critical infrastructures: Statistical analysis of power grid spectral clustering and post-contingency vulnerability metrics. *Renew. Sustain. Energy Rev.* 159, 112185. <https://doi.org/10.1016/j.rser.2022.112185>
- Rose, A., Casler, S., 1996. Input–Output Structural Decomposition Analysis: A Critical Appraisal. *Econ. Syst. Res.* 8, 33–62. <https://doi.org/10.1080/09535319600000003>
- Santos, J., Roquel, K.I.D.Z., Lamberte, A., Tan, R.R., Aviso, K.B., Tapia, J.F.D., Solis, C.A., Yu, K.D.S., 2023. Assessing the economic ripple effects of critical infrastructure failures using the dynamic inoperability input-output model: a case study of the Taal Volcano eruption. *Sustain. Resilient Infrastruct.* 8, 68–84. <https://doi.org/10.1080/23789689.2022.2127999>
- Sarkar, B.D., Gupta, L., 2023. Analyzing the impact of Russia-Ukraine crisis on the Indian economy using input-output modeling. *J. Glob. Oper. Strateg. Sourc.* ahead-of-print. <https://doi.org/10.1108/JGOSS-08-2022-0085>
- Schaefer, Rob, 2017. schae234/powerlaw.
- Schrijver, C.J., Dobbins, R., Murtagh, W., Petrinec, S.M., 2014. Assessing the impact of space weather on the electric power grid based on insurance claims for industrial electrical equipment. *Space Weather* 12, 487–498. <https://doi.org/10.1002/2014SW001066>

- Schulte, H., Moran, D., Lenzen, M., Cairns, I., Steenge, A., 2014. How severe space weather can disrupt global supply chains. *Nat. Hazards Earth Syst. Sci.* 14, 2749–2759. <https://doi.org/10.5194/nhess-14-2749-2014>
- Setola, R., De Porcellinis, S., Sforna, M., 2009. Critical infrastructure dependency assessment using the input–output inoperability model. *Int. J. Crit. Infrastruct. Prot.* 2, 170–178. <https://doi.org/10.1016/j.ijcip.2009.09.002>
- Singh, A.K., Bhargawa, A., Siingh, D., Singh, R.P., 2021. Physics of Space Weather Phenomena: A Review. *Geosciences* 11, 286. <https://doi.org/10.3390/geosciences11070286>
- Soon, S., Tiong, R., Lin, J., Tai, K., 2019. Modelling critical infrastructure network interdependencies and failure. *Int. J. Crit. Infrastruct.* 15, 1. <https://doi.org/10.1504/IJCIS.2019.10016804>
- Sprintson, M., Oughton, E., 2023. The contribution of US broadband infrastructure subsidy and investment programs to GDP using input-output modeling. <https://doi.org/10.48550/arXiv.2311.02431>
- Sue Wing, I., Rose, A.Z., 2020. Economic consequence analysis of electric power infrastructure disruptions: General equilibrium approaches. *Energy Econ.* 89, 104756. <https://doi.org/10.1016/j.eneco.2020.104756>
- SWORM, 2023. IMPLEMENTATION PLAN OF THE NATIONAL SPACE WEATHER STRATEGY AND ACTION PLAN.
- SWORM, 2015. NATIONAL SPACE WEATHER STRATEGY.
- SWORM, NSTC, 2019. SWORM and national science and technology council.
- Taran, S., Alipour, N., Rokni, K., Hadi Hosseini, S., Shekoofa, O., Safari, H., 2023. Effect of geomagnetic storms on a power network at mid latitudes. *Adv. Space Res.* 71, 5453–5465. <https://doi.org/10.1016/j.asr.2023.02.027>
- Taylor, A.R.E., 2020. Space weather as a threat to critical infrastructure. *Roadsides* 3, 63–72.
- USGS, 2024. Geomagnetism - Data & Tools | U.S. Geological Survey [WWW Document]. URL <https://www.usgs.gov/programs/geomagnetism/data> (accessed 12.23.24).
- Wang, S., Dehghanian, P., Li, L., Wang, B., 2020. A Machine Learning Approach to Detection of Geomagnetically Induced Currents in Power Grids. *IEEE Trans. Ind. Appl.* 56, 1098–1106. <https://doi.org/10.1109/TIA.2019.2957471>
- Webb, D.F., Howard, T.A., 2012. Coronal Mass Ejections: Observations. *Living Rev. Sol. Phys.* 9, 3. <https://doi.org/10.12942/lrsp-2012-3>
- Wu, T., You, Z., Gong, M., Cheng, J., 2021. Star Wars? Space Weather and Electricity Market: Evidence from China. *Energies* 14, 5281. <https://doi.org/10.3390/en14175281>
- Xue, D., 2023. Evaluating space weather effects of communication blackouts, GNSS-based navigation and surveillance failure, and cosmic radiation on air traffic management.
- Xue, D., Yang, J., Liu, Z., Yu, S., 2023. Examining the Economic Costs of the 2003 Halloween Storm Effects on the North Hemisphere Aviation Using Flight Data in 2019. *Space Weather* 21, e2022SW003381. <https://doi.org/10.1029/2022SW003381>
- Younas, W., Khan, M., Amory-Mazaudier, C., Amaechi, P.O., 2022. Ionospheric Response to the Coronal Hole Activity of August 2020: A Global Multi-Instrumental Overview. *Space Weather* 20, e2022SW003176. <https://doi.org/10.1029/2022SW003176>
- Zhang, J.J., Yu, Y.Q., Chen, W.Q., Wang, C., Liu, Y.D., Liu, C.M., Liu, L.G., 2022. Simulation of Geomagnetically Induced Currents in a Low-Latitude 500 kV Power Network During a Solar Superstorm. *Space Weather* 20, e2021SW003005. <https://doi.org/10.1029/2021SW003005>
- Zhao, Z., 2019. Economic Effects of Solar Activity: Evidence from Canada. Major Pap.
- Zorn, C., Pant, R., Thacker, S., Shamseldin, A.Y., 2020. Evaluating the Magnitude and Spatial Extent of Disruptions Across Interdependent National Infrastructure Networks. *ASCE-ASME J Risk Uncert Engng Sys Part B Mech Engrg* 6. <https://doi.org/10.1115/1.4046327>

Appendix

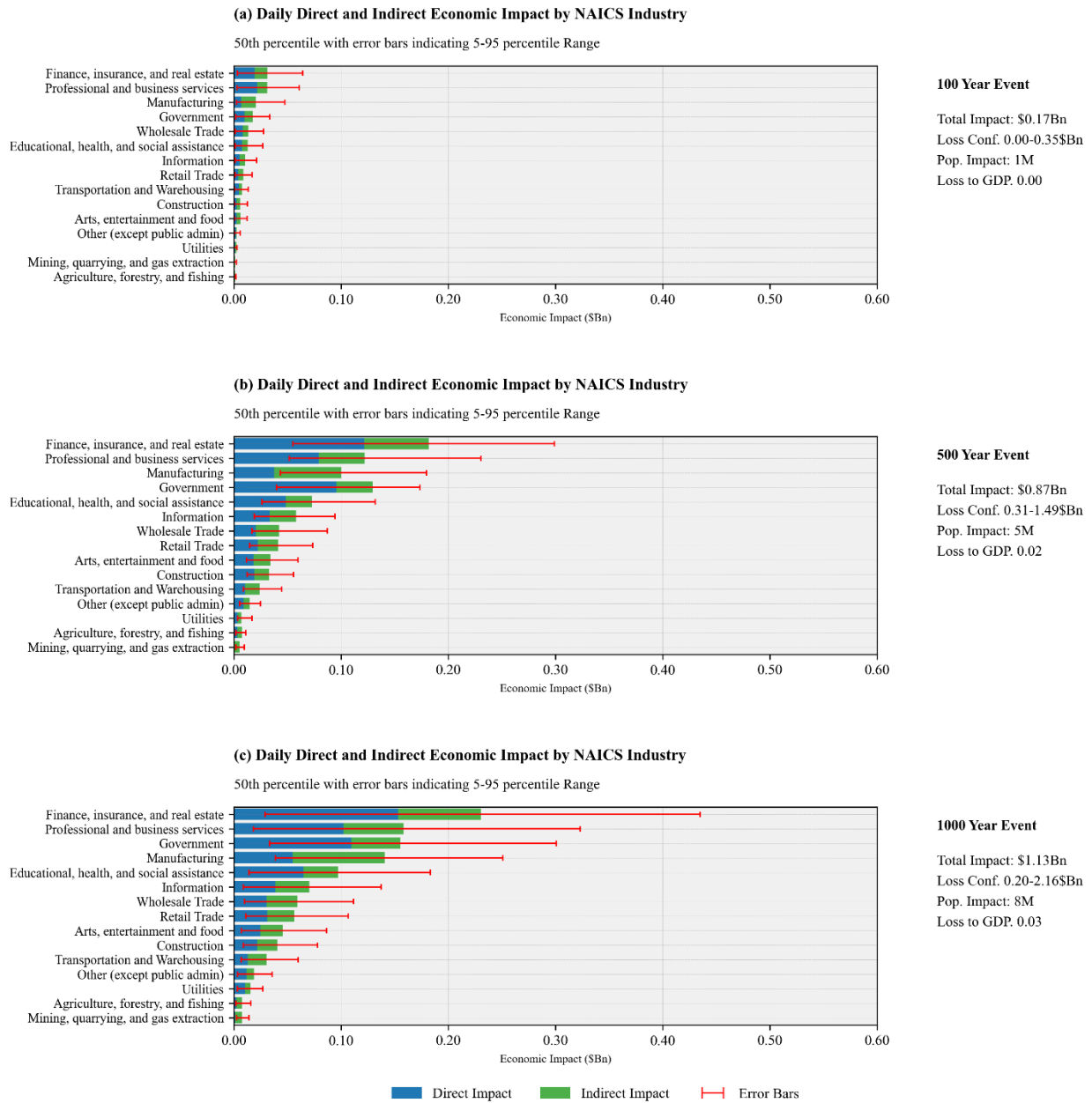


Figure A 1. Industrial breakdown of direct impacts from supply chain disruptions due to space weather using NERC thermal heating threshold of 100 A.

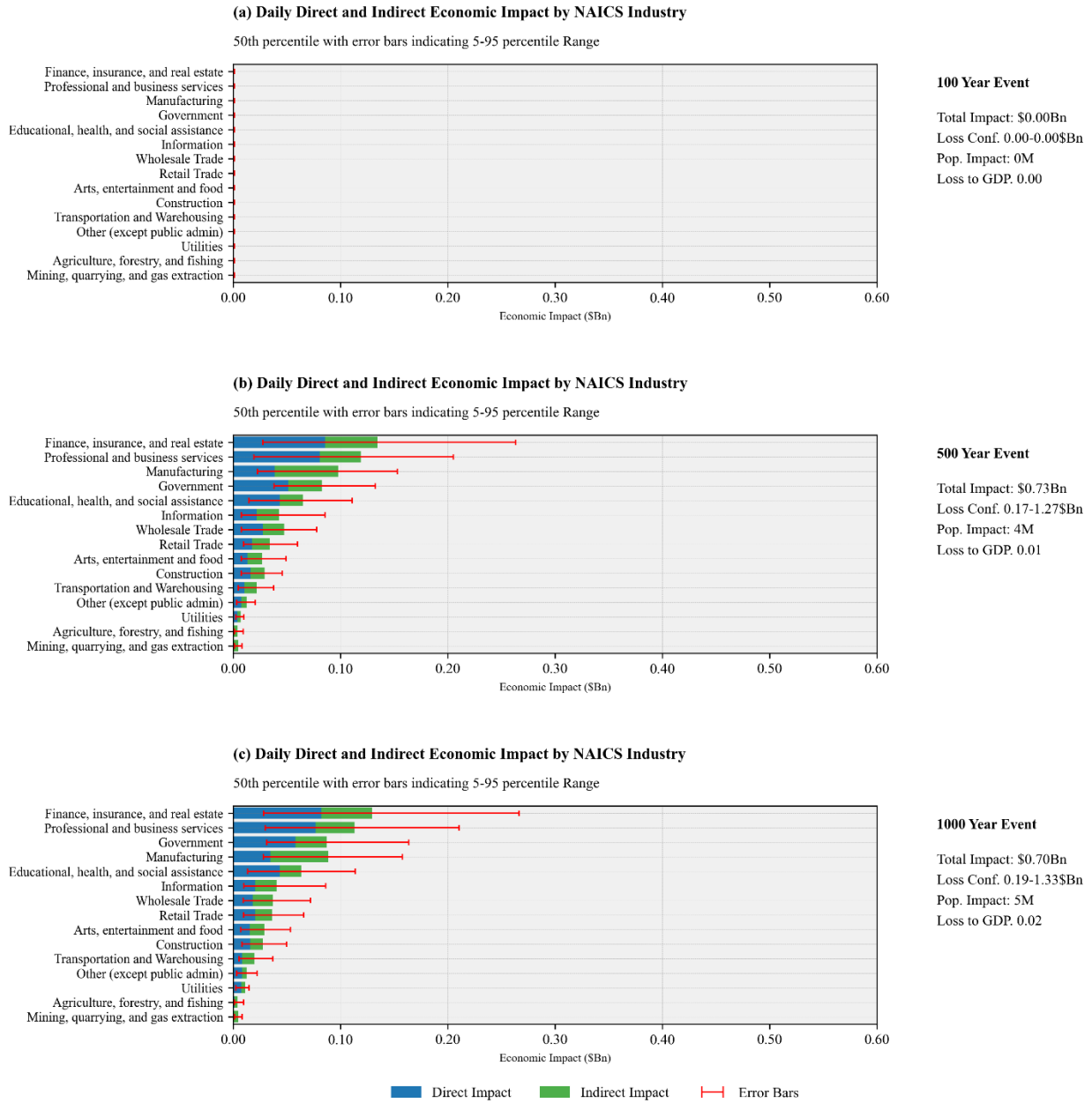


Figure A 2. Industrial breakdown of direct impacts from supply chain disruptions due to space weather. For transformers recording GIC above the NERC 125 A threshold, stochastic Monte Carlo simulation was used to derive the 2.5th, 50th, and 95th percentiles of direct impact within the cumulative distribution. The Ghosh model was then applied to estimate gross value-added losses across this investigated range.

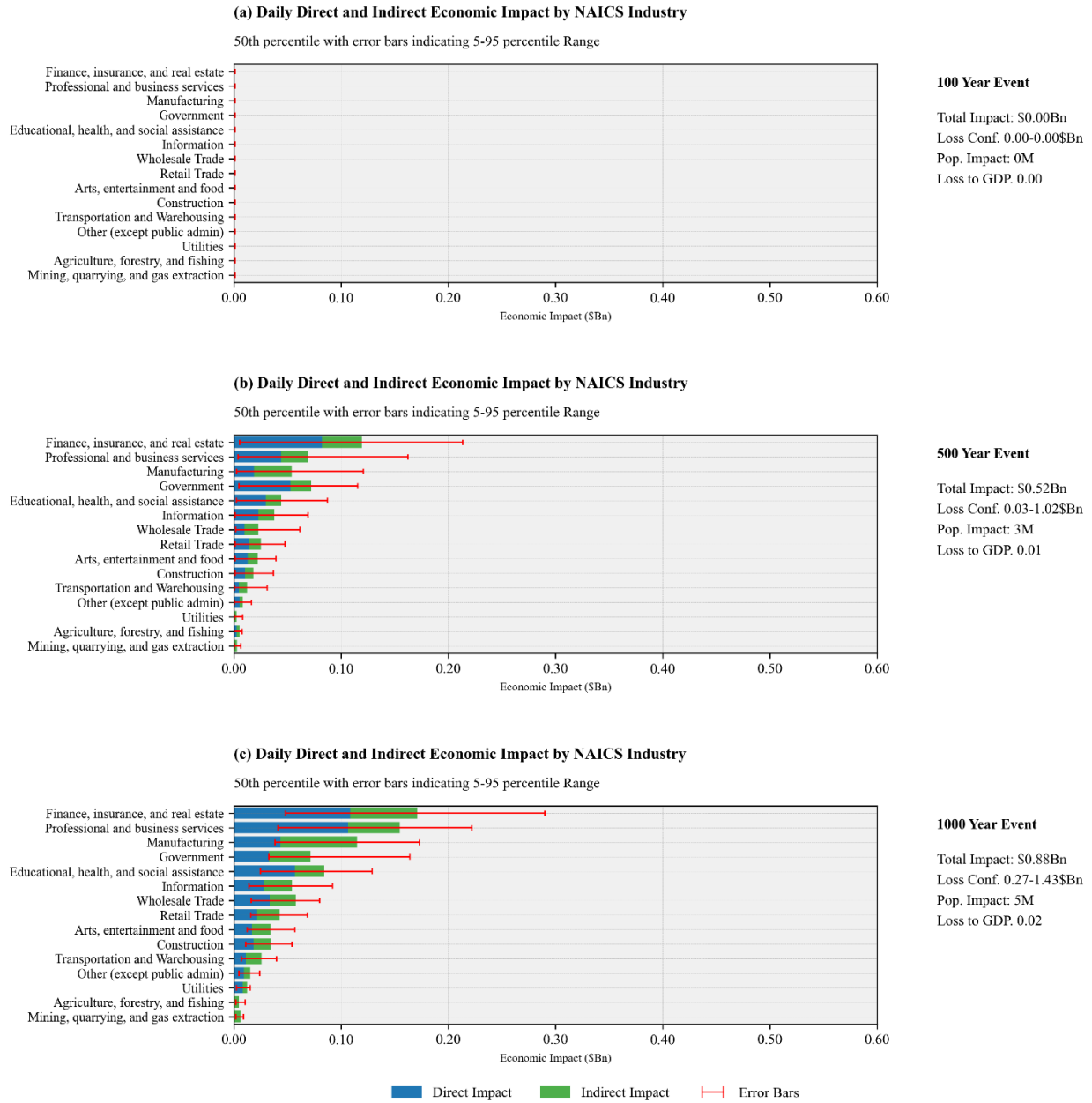


Figure A 3. Industrial breakdown of direct impacts from supply chain disruptions due to space weather. For transformers recording GIC above the NERC 150 A threshold, stochastic Monte Carlo simulation was used to derive the 2.5th, 50th, and 95th percentile